CHALMERS
UNIVERSITY OF TECHNOLOGY

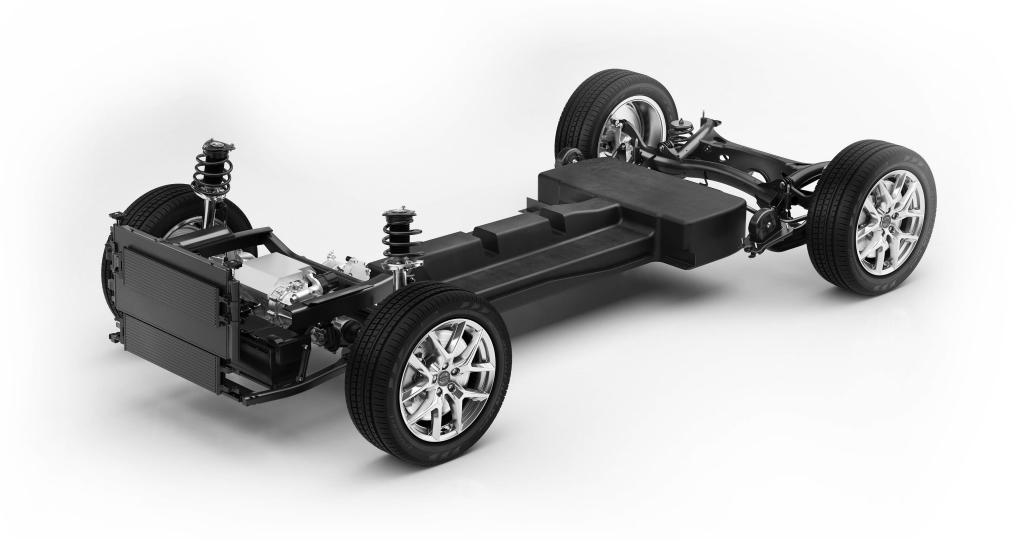

Model Predictive Control for the Thermal System of an Electric Vehicle

Analysis of a Model Predictive Control for WLTP Drive Cycle

Master's Thesis in Automotive Engineering

DAVID GRIMM

Department of Mechanics and Maritime Sciences
CHALMERS UNIVERSITY OF TECHNOLOGY
Gothenburg, Sweden 2019

Master's thesis 2019:NN

Model Predictive Control for the Thermal System of an Electric Vehicle

Analysis of a Model Predictive Control for WLTP Drive Cycle

DAVID GRIMM

CHALMERS
UNIVERSITY OF TECHNOLOGY

Department of Mechanics and Maritime Sciences
Division of Vehicle Engineering and Autonomous Systems
Chalmers University of Technology
Gothenburg, Sweden 2019

Model Predictive Control for the Thermal System of an Electric Vehicle
Analysis of a model predictive control for WLTP drive cycle
DAVID GRIMM

© DAVID GRIMM, 2019.

Supervisor: Monica Johansson, Volvo Cars
Examiner: David Sedarsky, Department of Mechanics and Maritime Sciences

Master's Thesis 2019:NN
Department of Mechanics and Maritime Sciences
Division of Vehicle Engineering and Autonomous Systems
Chalmers University of Technology
SE-412 96 Gothenburg
Sweden
Telephone +46 31 772 1000

Cover: CMA Battery Electric Vehicle Technical Concept Study - Source Credits: Volvo Car Group, https://www.media.volvocars.com/.

Typeset in LaTeX
Printed by [Name of printing company]
Gothenburg, Sweden 2019

Model Predictive Control for the Thermal System of an Electric Vehicle
Analysis of a Model Predictive Control for WLTP Drive Cycle
Industrial Supervisor: Monica Johansson, at Volvo Cars, Gothenburg
Master's Thesis in Automotive Engineering
DAVID GRIMM
Department of Mechanics and Maritime Sciences
Chalmers University of Technology

Abstract

With the continually increase of the global temperature and the CO_2 level in the atmosphere, stringent environmental policies for the automotive industry have been enacted to limit the growth and their consequences. 60.7% of the EU's transport sector's CO_2 is caused by passenger vehicles, constituting themselves as major contributor; electric vehicles (EVs) could decrease these emissions. Nevertheless, the competition is high and every advantage could be decisive. The range of EVs is critical and improving the energy efficiency of the thermal management could be the key.

New methods and control strategies have been developed over the last years and limiting factors like the processors available for vehicles have increased their performance massively. A theory which is common in slow processes like production plants has been redesigned in many academic investigations for the automotive usage and successfully tested. Predictive controllers have proven that they can de facto increase the energy efficiency and thus, increase the driving range of EVs.

The objective of this study is the design and analysis of a model predictive control (MPC) against classic control laws. The usage case will be the WLTP drive cycle which has been introduced recently as a more realistic drive cycle. Additionally, the WLTP will be modified by high demanding constant speed scenarios and increased in duration in order to reach thermal critical points. The test environment will provided by an interface model with Simulink and GT-SUITE; the control is based on Simulink whereas a cooling system of a battery-electric vehicle is created in the GT-SUITE. Consequently, the results of the simulation will be of high quality as the GT-SUITE model is established on real-life test data.

A method has been developed to connect multiple linear MPCs with the nonlinear GT-SUITE model. The MPC indicates a very high potential and could reduce the energy consumption by 59.29% for the modified WLTP, enhancements of this magnitude are not uncommon in research papers. However, tests with real-life applications need to be carried out to confirm these results.

Keywords: model predictive control, electric vehicle, WLTP, thermal management.

Acknowledgements

This work was carried out for the Division of Vehicle Engineering and Autonomous Systems at Volvo Cars. I would like to thank my supervisor Monica Johansson from Volvo Cars and my examiner David Sedarsky for their support throughout the thesis work. I also want to thank Yashasvi Nandivada for all the discussions and suggestions. I am also grateful for the essential input from Varun Venkatesh, Samuel Swedenborg and Sam Gullman for GT-SUITE. Last but not least, I want to thank Bhavani Burugu for her help to develop the interface model.

David Grimm, Gothenburg, June 2019

Nomenclature

Acronyms

MPCDESIGNER	Model Predictive Control Toolbox
SYSID	System Identification Toolbox
A/C	Air-conditioning system
$A/C-R$	Air-conditioning/refrigeration system
amb	Ambient
avg	Average
bat	Battery
BEV	Battery-electric vehicle
BTM	Battery thermal management
ECU	Engine control unit
ED	Electric-drive
EPA	United States Environmental Protection Agency
EU	European Union
EV	Electric vehicle
$init$	initial
$M-WLTP$	Modified WLTP
max	Maximum
$MIMO$	Multiple-input multiple-output
min	Minimum
MPC	Model predictive control
$NEDC$	New European Drive Cycle
$NYCC$	New York City Cycle
OEM	Original Equipment Manufacturer
PID	Proportional–Integral–Derivative controller
QP	Quadratic programming method
rad	Radiator

$SISO$	Single-input single-output
ss	State-space model
$UDDS$	Urban Dynamometer Driving Schedule
$V2I$	Vehicle-to-infrastructure
$V2V$	Vehicle-to-vehicle
$V2X$	Vehicle-to-everything
veh	Vehicle
$WLTP$	World-wide harmonized light vehicles test procedure

Controller parameters and variables

α	Tracking parameter
δ	Weighting factor for predicted error
λ	Weighting factor for control increments
M	Control horizon
n	Drift disturbance
P	Prediction horizon
r	Reference
t_s	Sampling time
w	Reference trajectory

Model parameters and variables

A, B, C, D, K	Constant coefficient matrices
e	White noise
k	Time step
t	Time instant
u	Input
x	State
y	Output

Symbols

Δ	Difference
$\dot{m}$	Mass flow
$\dot{Q}$	Heat flow rate
$\hat{\cdot}$	Expected value
C_p	Specific heat capacity
C_{nom}	Nominal capacity
C_{th}	Thermal heat capacity

I	Current
l	Level
m	Mass
n	Number of experiments
P	Power
p	Parameters
Q	Heat
R	Resistance
SoC	State-of-charge
T	Temperature
U	Energy
v	Speed
W	Work
z^{-1}	Backward shift operator

Contents

Abstract **v**

Acknowledgements **vi**

Nomenclature **vii**

List of Figures **xv**

List of Tables **xvii**

1 Introduction **1**
1.1 Background . . . 1
1.2 Scope . . . 2
1.3 Motivation . . . 3
1.4 Limitations . . . 3
1.5 Classic and Predictive Control Strategies . . . 4
1.6 Outline . . . 5

2 Theory **7**
2.1 Literature review . . . 7
2.2 Battery-Electric Vehicle . . . 10
2.2.1 Chiller . . . 12
2.2.2 Radiator . . . 12
2.2.3 Thermal Battery Model . . . 13
2.3 Thermal Modes . . . 14
2.3.1 Chiller Cooling . . . 14
2.3.2 Radiator Cooling . . . 15
2.3.3 Idling . . . 16
2.4 Worldwide harmonized light vehicles test procedure - WLTP . . . 16
2.5 MPC . . . 18
2.5.1 Prediction Model . . . 18
2.5.1.1 Process Model . . . 19
2.5.1.2 Disturbance Model . . . 19
2.5.2 Objective Function . . . 19
2.5.3 Obtaining Control Law . . . 20

3 Methodology **23**
3.1 Workflow . . . 23
3.2 Data Acquisition . . . 24
3.2.1 Parameter Identification . . . 24
3.2.2 Design of Steady-State Experiments . . . 25
3.2.3 Simulation . . . 25
3.3 System Identification Toolbox . . . 26
3.4 Model Predictive Control Toolbox . . . 29
3.5 GT-SUITE/Simulink Interface . . . 31
3.5.1 Fine-Tuning of MPC . . . 32
3.5.2 Classic Control . . . 32

4 Results **33**
4.1 Temperature . . . 33
4.2 Thermal Modes and Input Signals . . . 34
4.3 Energy Consumption . . . 35
4.4 Analysis . . . 36

5 Conclusion **37**

6 Future Work **39**

Bibliography **41**

List of Figures

1.1 Left: global surface temperature relative to 1951-1980 average temperatures, 1880-2019; right: CO_2 levels measured at Mauna Loa Observatory in Hawaii with average seasonal cycle removed, 2005-2019. 1
1.2 Share of CO_2 emission from fuel combustion by sector or source in EU. 2
1.3 *ngrams* search for control techniques. 3
1.4 MPC. 4

2.1 Left: thermal management system of a hybrid; right: Tesla Model 3 thermal management system from A2mac1. 10
2.2 Architecture of the investigated battery-electric vehicle [24]. . . . 11
2.3 Left: cycle of vapor-compression refrigeration; right: fictive pressure-volume diagram for refrigeration cycle. 12
2.4 Simplified radiator sketch. 13
2.5 Illustration how the CO_2 goal for 2021 is based on NEDC with absolute value of $95 g/km$, while after 2021 a percentage CO_2 reduction applies, relative to WLTP. 17
2.6 M-WLTP drive cycle with a cycle length of $6600 s$. 18
2.7 A generic model predictive control loop. 18
2.8 Trajectory of reference signal. 20

3.1 Project workflow. 23
3.2 Relevant parameters from M-WLTP data. 24
3.3 Chosen cooling system of BEV in GT-SUITE. 25
3.4 Left: derivative of battery temperature; right: preprocessing of input/output data. 26
3.5 State-space estimation via sysID. 27
3.6 Selection of plant model in mpcDesigner. 29
3.7 Step signal on MPC in mpcDesigner. 30
3.8 MPC exported to Simulink. 31
3.9 GT-SUITE/Simulink interface model. 32

4.1 Battery temperature. 33
4.2 Left: ED component temperature; right: temperature from temperature sensor. 34

4.3 Left: ED circuit pump speed; right: battery circuit pump speed. . 34
4.4 Left: thermal modes; right: fan speed. 35
4.5 Left: energy consumption of complete WLTP; right: energy consumption of cut WLTP. 35
4.6 Comparison of drive cycles. 36

List of Tables

2.1 WLTP/NEDC comparison table. 16
2.2 M-WLTP initialization data. 17

4.1 Violation of target temperature. 33
4.2 Energy consumption. 36

1
Introduction

1.1 Background

With the rise of the global temperature accompanied by increasing CO_2 levels (see figure 1.1), political bodies like the European Union (EU) agreed on a new legislation for car manufactures (OEMs) to reduce their fleet CO_2 emissions[1]. The direct impact of CO_2 on the global temperature is undeniable and immediate actions are necessary[3]. In 2014, the transport sector was responsible for around 27.55% of the EU's CO_2 emission with a growing tendency (figure 1.2).

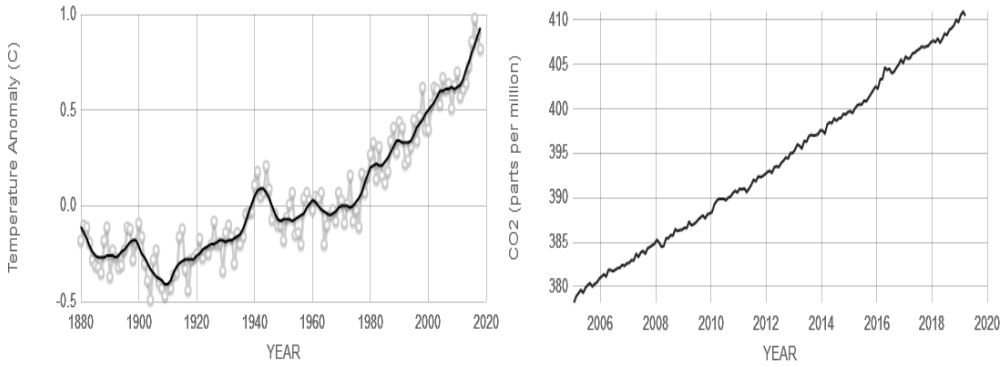

Figure 1.1: Left: global surface temperature relative to 1951-1980 average temperatures, 1880-2019; right: CO_2 levels measured at Mauna Loa Observatory in Hawaii with average seasonal cycle removed, 2005-2019[2].

Around 60.7% of the CO_2 emissions were caused by passenger vehicles, making it the major contributor from the transport sector. The new legislation targets to reduce the CO_2 emission by 15% in 2025 and by 35% in 2030 compared to real-world data measured from vehicles sold in 2020[5]. As a base, the Worldwide harmonized light vehicles test procedure (WLTP) was developed to provide authenticity of the data. This new drive cycle takes more realistic driving conditions into account. OEMs develop as a result alternative drivetrains to be able to meet these new requirements.
Battery-electric vehicles (BEVs) are CO_2-free in the eyes of this legislation and hence, are popular amongst OEMs and customers[6]. Yet, a major concern is the lower range of current BEVs compared to conventional vehicles. By optimizing the battery consumption, the range can be increased.

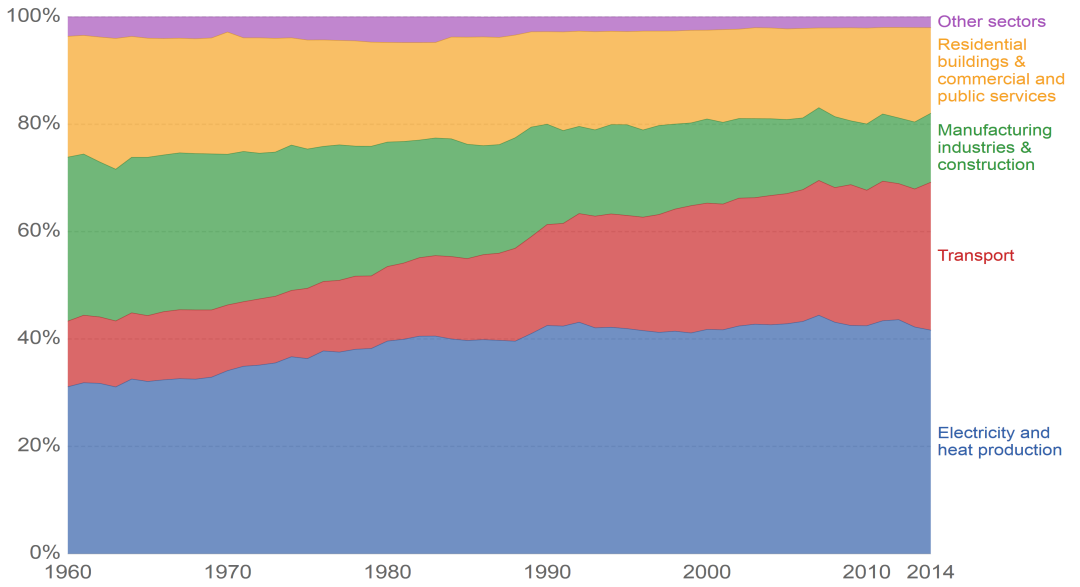

Figure 1.2: Share of CO_2 emission from fuel combustion by sector or source in EU[4].

The battery thermal management (BTM) of the electric powertrain consumes 6% to 10% of the battery energy and provides room for improvement[46]. Nevertheless, it is crucial to keep the battery cool to not impair its durability and range. This asks for an energy efficient and smart BTM of the electric powertrain. Since the thermal components are not mechanically but electrically controlled, the architecture of electrified vehicles offers more degrees of freedom for the thermal management.
Currently, most systems rely on a bang-bang control or a PID-control. These reacting control laws are robust and simple but cause often over- or undershooting of the target which results into a higher energy consumption. An alternative is the model predictive control (MPC).
Since the 1980s, it is widely used in the process industry and today, with higher computational power and optimized models, it became more popular in the automotive industry. Designing a model predictive control for the cooling of the electric powertrain could offer an efficiency advantage and decrease the energy consumption. There are various scientific papers focusing on predictive controllers and comparing them to classic control strategies.

1.2 Scope

The objective is to design a model predictive control for the battery thermal management of a BEV. Its performance will be evaluated against a classic control strategy. A drive cycle with data from Volvo Cars frames the base of this work and an interface model between Simulink and GT-SUITE will be developed to provide the simulations. The model in GT-SUITE is provided by Volvo

Cars and will also be adjusted. The battery-electric vehicle will be inspired by literature and redesigned for this task.

1.3 Motivation

Classic control laws are to a certain extent limited in their abilities. Control theory provides solutions which allow smarter approaches and with today's hardware are feasible for real-life applications. Figure 1.3 indicates the growing academic interest in MPCs compared to other controls.

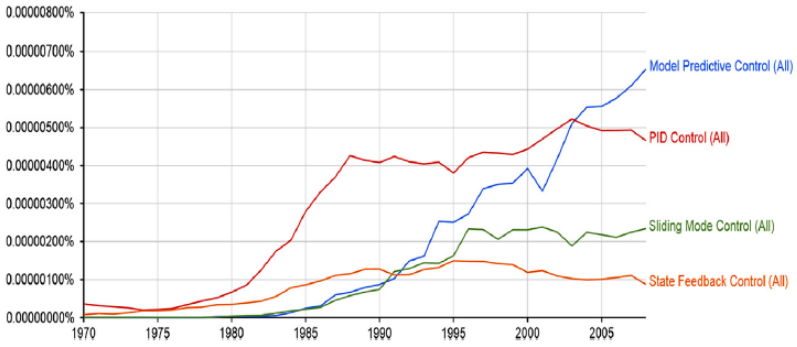

Figure 1.3: *ngrams*[1]search for control techniques[8].

This investigation will deliver a comparison of a BTM established on classic control and on predictive control. The capability of the tool used, the GT-SUITE/Simulink interface model, will be of interest as well. It could prove itself as a powerful tool in order to design controllers in a realistic simulation.

1.4 Limitations

The focus of this work is on the model predictive control of a BEV. The classic-controlled BTM will undergo a shorter development time. Consequently, it might not have the same finesse as the model predictive control. The GT-SUITE model of the BEV by Volvo Cars will be adjusted and calibrated for this purpose. The conditions of the environment and the vehicle components are set and the results only apply on these predefined conditions. Additionally, the GT-SUITE model and the drive cycle data limit the scope by non-availabilities of certain parameters and models. For example, the effect of state-of-charge (SoC) on the battery is not integrated in the GT-SUITE model as well as the thermal models of the electric drive components. Hence, the focus lies on the thermal model of the battery.

[1]Google Ngram Viewer shows the frequency of character strings discovered in published papers between 1500 and 2008[47]

1.5 Classic and Predictive Control Strategies

To this day, most applications will be controlled by classic control laws. The simplicity and still, the effectiveness contribute to their popularity. This section will introduce a description of the bang-bang or on/off controller, the proportional–integral–derivative controller (PID), and the model predictive controller. The latter will also be explained in detail in chapter 2.
Bang-bang controllers change between two conditions which is triggered by a threshold. Fans or thermostats often rely on this control[7]. The PID is more sophisticated and calculates an error between a target value and a measured variable. The proportional, integral and derivative parts of the controller determine a correction which is applied to regulate the system. It is a common practice for cruise control.
Both traditional controllers are still very prevalent even though they are limited. They cannot handle constraints, dynamic systems or multi-input-multi-output systems without creative approaches of control engineers[8][9][10].
On the other hand, the MPC is capable of handling multiple constraints and signals as well as optimizing for multiple references. It can manage dynamics of a system and react effectively. This is because it works with a mathematical model of the plant as the name "model predictive control" suggests. The process is visualized in figure 1.4.

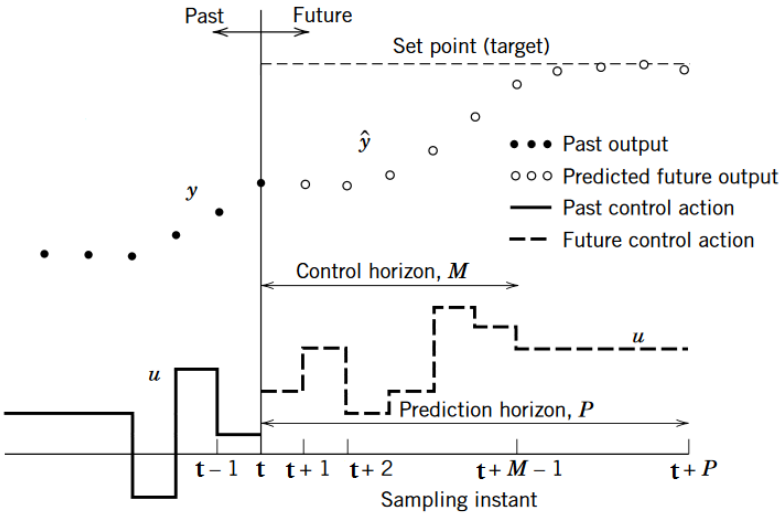

Figure 1.4: MPC[11].

The control engineer sets a prediction horizon P and control horizon M with $M < P$. P is the time period the MPC can predict accurately, M is the time period where the MPC applies changes to input u.
The MPC calculates at time instant k for each time step $j = 1$ the control period M which contains the set of values of u that can help the plant's output y to reach the set point in the prediction time P. It chooses the path according to a

cost function which is given by the control engineer. Another aspect is that for each k, this procedure is executed. This makes the MPC very efficient but also computational intense[12][13][14].

1.6 Outline

The work will be presented in the following manner. The theory, chapter 2, is split into a literature review and a technical review. The first focuses on different approaches of designing and implementing an MPC in the automotive industry. The context is either BTM efficiency or improvement of diesel emissions. The latter presents the architecture of a BEV with the components of interest, thermal battery model, radiator, chiller, and the modified WLTP drive cycle. Then the thermal battery modes and the model predictive control will be elucidated. The theory is followed by the methodology, chapter 3. The project workflow with all steps from building the plant model to creating the MPC are described. Chapter 4 will show the results of this study and analyze them. Finally, a conclusion will be drawn and future works will be proposed in chapter 5.

2
Theory

In the theory section, a literature review is conducted with a focus on model predictive control. Examples from the automotive industry are given as well as different MPCs, linear or nonlinear. Afterwards, the architecture of a battery-electric vehicle will be presented with the cooling circuit and relevant components. The use case, the drive cycle, follows with the thermal battery modes visualized and the logics shown as pseudo-algorithms. The model predictive control will complete the theory section.

2.1 Literature review

In the automotive industry, control strategies are limited by the computational power of the engine control unit (ECU) and by the state of the art in control engineering. With major improvements in both fields and increasing vehicle complexity, the classic heuristic approach is not suitable anymore and a more systematic approach should be pursued.
In the slow but complex process industry, MPC enjoys great popularity and has been widely used since the mid 1980s. Recently, the automotive industry has started to investigate this strategy and its applicability. In [15], the authors design a discrete MPC to reduce the energy consumption of an automotive air-conditioning/refrigeration (A/C-R) system and compare it to an on/off control strategy. With the A/C-R system being highly nonlinear, the system model has been linearized and discretized and a finite horizon optimization problem has been defined. These steps are necessary in order to accomplish real-time performances since a nonlinear model's computational demand would be too high. The case study with varying heating loads on the A/C-R system shows that for high demands the MPC improves the efficiency but that for lower demands the conventional control is less energy-consuming. Combining both strategies into a hybrid form can reach improvements of 15%.
In [16], the focus is on the fan control for automotive applications. A cooling circuit of a BEV consisting of an electric motor, heat exchanger, and two connecting pipes is considered. The plant is derived with a linear part of the motor and pipes, and a nonlinear part of the heat exchanger. The non-linearity is addressed by a PI-observer[17]. The authors in [16] state that according to affinity laws for pumps and fans, a higher temperature delta and lower mass flow are more desirable than the opposite. Rising the mass flow by 10% results into a

33% higher power demand since $\frac{P_1}{P_2} = (\frac{\dot{m}_1}{\dot{m}_2})^3$. Hence, a variable fan speed can be crucial.
The comparison proceeds between an MPC and a common control with four discrete fan speed levels. In their use case, an energy reduction of almost 50% could be achieved and the MPC's oscillations around the reference temperature is extremely low. Additionally, real-time experiments have been positively conducted and showed promising results.
In [8], the authors state that the development time of a control strategy can benefit from a systematic technique. Even though an MPC is more complicated to establish, it can handle individual restraints and optimize for the use case, in here a diesel engine.
A system identification method on the diesel engine was applied to find a linear approximation. First, a design of experiment with varying actuator values on a test cell was carried out. With the input and output data all single components are identified. Then, the components are united and steady-state identifications are performed with accuracy intervals of 10% and 20%. A high correlation between the nonlinear system and measured test-data is crucial for a good control. Last, the dynamics of the system need to be determined for a realistic engine behaviour. This allows to design a mulitple MPC. Distinguishing between different engine speeds and fuel injection quantities provides the differentiation of the multiple linear models.
With these models the linear MPCs can be designed. Now the multiple linear MPCs can be connected to the nonlinear plant and a logic selects according to engine speed and fuel injection quantity the correct MPC. The control strategy was installed on a light duty diesel engine and the EPA Urban Dynamometer Driving Schedule served as drive cycle. The results are affirmitive and the constraints on the engine actuators were all obeyed. The authors state that a more low-emission oriented control strategy can be followed and they conclude MPCs will find more applications in the industry.
Amini et al.[18] compares a single-layer and a two-layer MPC for battery thermal and energy management with a traditional rule-based control. Focusing on energy-optimization for connected BEVs, savings of 2.8% to 7.9% are achievable. Having a vehicle-to-vehicle and/or vehicle-to-infrastructure (V2V/V2I) environment provides information to increase energy efficiency[19]. In this study, the vehicle speed is known and implemented in the MPCs. Approximating the battery as one mass m_{bat} allows for following expression[20]:

$$\dot{T}_{bat}(t) = \frac{(I_{bat}^2 R_{bat} + \dot{Q})}{m_{bat} C_{th,bat}} \tag{2.1}$$

with battery temperature T_{bat}, current I_{bat}, internal resistance R_{bat}, heat capacity $C_{th,bat}$, and the heat flow rate $\dot{Q}$ as the single input to the control. The electric model's definition follows as a function of the state of charge SoC with I_{bat} and the nominal capacity of the battery C_{nom}:

$$\dot{SoC} = -\frac{I_{bat}(t)}{C_{nom}} \tag{2.2}$$

With the Euler forward method, the thermal and electric sub-models are discretized to allow to build the MPC.
Amini et al. aim on minimizing the required power for cooling the battery in the cost function and set upper and lower boundaries on the battery temperature. With the battery being a slow thermal model, the prediction horizon is relatively high. Hence, the single-layer MPC is tested with a prediction horizon of $10, 60, 120, 180s$ against the rule-based control.
Simulating the EPA Urban Dynamometer Driving Schedule (UDDS), all four controls could reduce the energy consumption by 4.5% to 5.3%. Yet, only the two latter controls could reduce a boundary violation compared to the classic control. Additionally, the average computational time was $0.75, 2.22, 6.24, 10.78s$ per iteration. With a sampling time of $t_s = 1s$, a real-time application is not feasible.
Amini et al. assume that the improvements might not rely on accurate vehicle speed data. Also, accurate vehicle speed data for a long time period is not absolutely reliable since there are many factors influencing it. Methods from [21][22] are applied where the traffic speed is determined by the cellular infrastructure, and GPS information of phones. Using the traffic speed instead results into an improvement of 3.9%.
As a next step, the authors propose the two-layer MPC with a scheduling layer MPC and a piloting layer MPC. A scheduling layer MPC with a long prediction horizon optimizes for $\dot{Q}$ and delivers T_{bat} and SoC to the piloting layer MPC with a short prediction horizon. The scheduling layer MPC is fed with the traffic speed whereas the piloting layer MPC can utilize an accurate estimation of the vehicle speed since the time period is short. Furthermore, the possible error of the calculated battery temperature from the vehicle speed and from the traffic speed is considered by an algorithm. This reduces the constraint violation of the battery temperature by 13%, costs as a consequence 1% more energy with the UDDS drive cycle.
The authors simulate the New York City Cycle (NYCC) as well and compare the two-layer MPC to the rule-based controller at initial conditions $T_{bat} = 35°C$ and $T_{bat} = 39°C$. The upper limit is $\overline{T}_{bat} = 40°C$. For the UDDS, an improvement of 2.9% and 2.8% are achieved whereas the MPC manages a consumption decrease of 7.7% and 7.9% with the NYCC.
The greater decrease is linked to the less demanding drive cycle characteristics. Equally important is that a significant reduction of the computational time could be achieved. Amini et al state a real-time application is now practical.
In [23], a MIMO-system of a thermal management system for an electric vehicle is developed. The authors untie it into SISO-systems and control it via PI-controls. In a follow-up study of the authors[24], a nonlinear MPC is designed to control the cabin's temperature and the superheat temperature.
In the former investigation, the PI-control's interaction caused problems as the constraints were interfering with each other; oscillations, over- and undershootings were the result. The nonlinear MPC is capable of handling multiple constraints and optimize for multiple outputs.

The comparison between the nonlinear MPC and the PI-controllers proved this theory very well. Faster and smoother reactions were achieved for step inputs. The authors conclude that this behaviour is also an indicator for a better energy efficiency since high performance demands are being avoided with the predictive control of the MPC. Yet, Fischer et al. states that the development is challenging and the real-time application is not fully possible. A further study needs to be performed. The battery temperature is excluded in the follow-up study [24] because of the complexity unlike in the prior study [23]. Other points of improvement are the real-time applicability with the run of a drive cycle, and the implementation in a vehicle.

2.2 Battery-Electric Vehicle

The object is a batter-electric vehicle. Car manufacturers are notoriously delicate about the interior life of their products in order to prevent the competition to benefit from their research and development. Thus, sources about the cooling system architecture from OEMs are rare and third parties like academic researches or supplier information have to be investigated. Fischer et al.[23] designed a hybrid vehicle where all heat sources and heat sinks are utilized to fulfill heating and cooling demands respectively, see left figure 2.1. The proposed concept consists of the electric-drive (ED) cooling circuit being connected via three-way valves to the battery cooling circuit which are likewise connected to the cabin cooling circuit. The thermal requests can each be met with either the ambient heat exchanger in the ED circuit, a radiator/fan, or a flow reversal in the heat pump of the AC-system, a chiller. A similar arrangement regulates the temperature of the Tesla Model 3, right figure 2.1. The battery and ED cooling circuits are connected via a complex valve system.

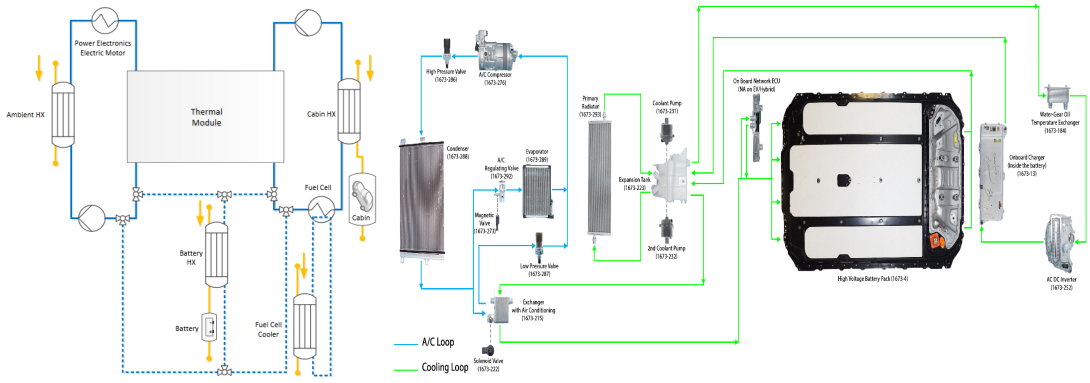

Figure 2.1: Left: thermal management system of a hybrid[23]; right: Tesla Model 3 thermal management system from A2mac1[50].

A solenoid valve and an exchanger with air conditioning on the bottom left ensure the link between the cooling loop and A/C loop; the cooling loop refers to the battery and ED cooling circuit, the A/C loop to the cabin cooling circuit.

Additionally, a heat exchange occurs in the expansion tank where the coolants of the battery and ED circuits flow through.
For the purpose of this study, an established arrangement from Fischer et al. [24] was selected. The layout of the vehicle is displayed in figure 2.2. The battery and ED cooling circuits can be connected via the 3/2 valves. The cabin cooling circuit will be neglected and merged with the battery cooling circuit which gives two circuits in total: battery and electric drive cooling circuit.

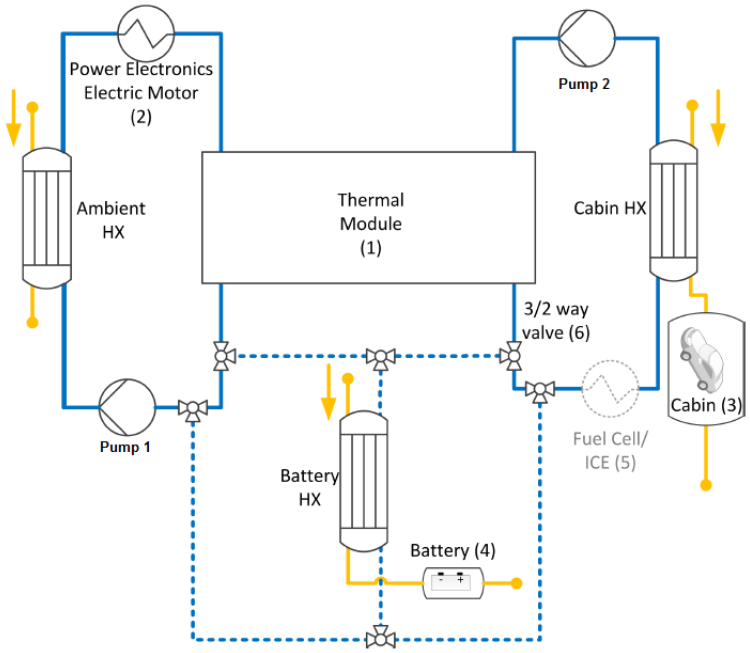

Figure 2.2: Architecture of the investigated battery-electric vehicle [24].

The valves are either fully opened or closed. Each circuit has a pump which regulates the mass flow of the coolant. Their operating speed range can move from 0% to 100% with two conditions. First, when both circuits are connected via the valves the pumps must operate at synchronized speeds to deliver equal mass flows. Second, a minimum coolant mass flow must be delivered to ensure that the components are fully temperate. This sets the minimum pump speed at 25%; analysis of GT-SUITE simulations provided this value and a safety coefficient was applied. In GT-SUITE, a thermal model of the battery is provided but not of the ED components which are presented as lumped block. However, the coolant's temperature in the ED cooling circuit can be used as substitution which shall not exceed a safe temperature limit. Worth mentioning is that the ED cooling circuit is usually warmer than the battery cooling circuit. The architecture enables three thermal scenarios: chiller cooling, radiator cooling, idling. The modes will be further elucidated in the theory chapter. Au contraire, the chiller's and the battery's thermal model's introduction follows here.

2.2.1 Chiller

The chiller is a device used for cooling a liquid through a vapor-compression refrigeration cycle, see figure 2.3. The refrigerant comes as vapor to the compressor and at constant entropy, it is compressed and exits as superheated vapor with about $+5°K$[24]. The superheated vapor moves through the condenser, first cooling and removing the superheat, then condensing the vapor into a liquid by removing additional heat at constant temperature and pressure. The liquid refrigerant passes via the expansion valve where its pressure drops sharply, allowing flash evaporation and auto-refrigeration of less than half of the liquid typically. This results in a reduced temperature and pressure mixture of liquid and vapor. The cold liquid-vapor mixture moves through the evaporator coil and is fully vaporized by cooling the warm air that is blown by a fan crosswise the evaporator coil[25][26][27][28][29][30].

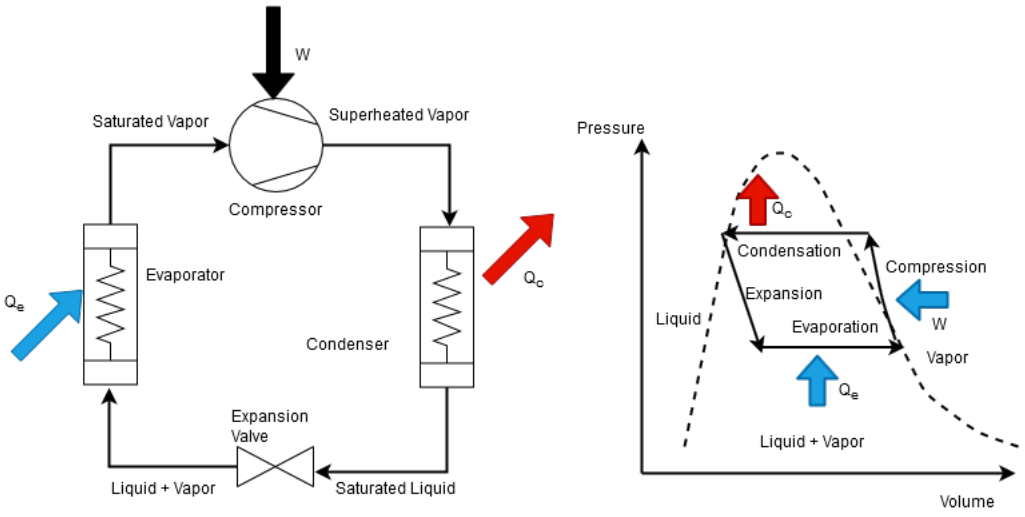

Figure 2.3: Left: cycle of vapor-compression refrigeration; right: fictive pressure-volume diagram for refrigeration cycle.

2.2.2 Radiator

As heat exchanger, enables the radiator the transfer of heat of the entering hot coolant to the surrounding air. It is connected via channels with the electric drive components and the battery as given in figure 2.2. The hot coolant $\dot{m}_{coolant}$ enters at the top of the radiator and flows through many parallel pipes[43]. Thereby, the hot coolant transmits its heat to the environment and exits cooled down at the bottom of the radiator (figure 2.4).

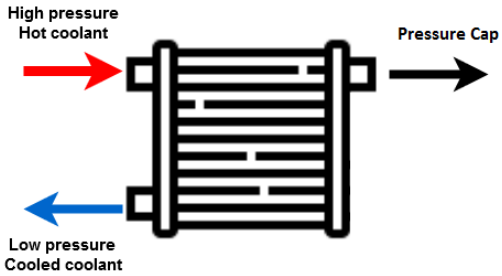

Figure 2.4: Simplified radiator sketch.

However, the radiator with the cooling circuit has a rather counter-intuitive working principle. If the speed of pump 1 is lowered, the coolant temperature from the ED circuit $T_{ED,out}$ increases since it has more time to pick up heat Q from the ED components. $T_{ED,out}$ is equal to $T_{rad,in}$ which enters the radiator and passes through it slower. With constant pump speeds, fan speed and ambient temperature T_{amb}, there is more exposure time to cool $T_{rad,in}$ until it exits the radiator. The radiator outlet temperature $T_{rad,out}$ will be closer to T_{amb}. The radiator inlet and outlet temperature difference ΔT_{rad} is greater and consequently the cooling potential as well. This is based on the first law of thermodynamics. The radiator can be considered a closed thermodynamic system: the matter in the system is constant but heat is exchanged. The first law of thermodynamics states for closed systems:

$$dU = \delta Q - \delta W \tag{2.3}$$

with the internal energy dU, the amount of energy added δQ by heating and the amount of energy lost δW due to work. The heat Q is

$$Q = \dot{m}_{coolant} C_{p,coolant} (T_{rad,in} - T_{rad,out}) \tag{2.4}$$

with the specific heat capacity $C_{p,coolant}$ of the fluid. When the conditions for the fan/radiator are constant, namely ambient temperature T_{amb}, fan speed v_{fan}, pump speed 1 $v_{pump,1}$ and 2 $v_{pump,2}$, the deliverable heat Q is constant as well. Contemplating equation 2.4, it becomes clear that if Q is constant, but $m_{coolant}$ decreases, the ΔT_{rad} has to increase[44][45]. Thus, a lower $T_{rad,out}$ can be achieved.

2.2.3 Thermal Battery Model

The development of a thermal control strategy requires a thermal battery model. Lithium-ion batteries are very common in the automotive industry due to their low self-discharging rate, high voltage, and high energy density compared to other batteries[31][32][33]. Their sensitivity towards extreme temperatures have also been studied; when high temperatures can lead to a risk of explosions or performance degeneration, low temperatures can decrease the capacity because of freezing electrolytes[34][35][36][37]. Consequently, an accurate model is essential. The lithium-ion battery consists of many materials with different heat capacities

which make it highly complex. For the use case, a state-space representation of the battery model is desired:

$$\begin{aligned} \dot{x} &= Ax + Bu \\ y &= Cx + Du \end{aligned} \tag{2.5}$$

The general state-space model consists of the state vector x, the output vector y, the input vector u and the constant coefficient matrices A, B, C, D. In order to develop a state-space representation of the battery, constant thermal conditions have to be set. In theory, all different materials and components of the litium-ion battery cause non-linearities. A reduced-order model [38] views the battery as a lumped mass m_{bat} with heat capacity $C_{th,bat}$ and proved itself as precise. A simple battery can be viewed as a single-input single-output system. The battery current I_{bat} effects the battery temperature T_{bat} as does the heat flow rate $\dot{Q}$; in case of cooling: $\dot{Q} < 0$.

$$\dot{T}_{bat}(t) = \frac{1}{m_{bat} C_{th,bat}} (I_{bat}^2 R_{bat} + \dot{Q}) \tag{2.6}$$

Here, $\dot{Q}$ is treated as input parameter to the system. It will be the parameter that will be controlled to influence the battery's temperature. A further step is the discretization of equation 2.7 via the Euler forward method with k being the time step and t the time instant:

$$T_{bat}(t+1) = f_{T_{bat}}(t) = T_{bat}(t) + k\dot{T}_{bat}(t) \tag{2.7}$$

This knowledge is important in order to run the correct simulation setup. The simulation's results will be used to construct the state-space model of a reduced-order battery[39].

2.3 Thermal Modes

The illustrated architecture (figure 2.2) enables three thermal scenarios for the battery: chiller cooling, fan cooling, idling. The equitable mode will be chosen by a logic; according to the battery temperature T_{bat}, the ED coolant temperature T_{ED}, the ambient temperature T_{amb}, and the temperature from the sensor T_{out} the logic selects the correct mode. The coolant's flow will be depicted below. Additionally, pseudo-algorithms will summarize the logic for each mode[48].

2.3.1 Chiller Cooling

There are two cases for chiller cooling. Both cases make use of the chiller as it is the most effective way to cool the components. First, the battery temperature is above a high critical battery temperature threshold $\overline{T}_{bat}$ and needs immediate cooling. The three-way valves close towards the warmer ED circuit, thus isolating the battery circuit. Second, the ED coolant temperature is above a high critical

ED temperature threshold $\overline{T}_{ED}$. If radiator cooling of the ED components is not sufficient and the temperature T_{out} is below $\overline{T}_{bat}$, the valves connect the battery and ED circuits and both pumps as well as the chiller run.

Algorithm 1 Chiller Cooling

```
1: if T_bat ≥ T̄_bat then
2:     Valves disconnect battery circuit from ED circuit
3:     Pump 2 is active
4:     Chiller is active
5: else
6:     if T_ED ≥ T̄_ED && T_out < T̄_bat then
7:         Valves connect battery circuit from ED circuit
8:         Pump 1 is active
9:         Pump 2 is active
10:        Chiller is active
```

2.3.2 Radiator Cooling

For radiator cooling, two cases exist as well. When the battery temperature is above a low critical battery temperature threshold $\underline{T}_{bat}$ and the temperature T_{out} is below $\underline{T}_{bat}$, then the valves connect the battery circuit with the ED circuit. The second case is when the ED temperature is above a low critical ED temperature threshold $\underline{T}_{ED}$, the battery temperature is below $\underline{T}_{bat}$ and the ambient temperature T_{amb} is below T_{out}. The flow is highlighted in figure **??**. The last condition indicates that radiator cooling is most effective in milder climates since this provides the largest temperature difference ΔT between coolant and surrounding.

Algorithm 2 Radiator Cooling

```
1: if T_bat ≥ T_bat && T_out < T_bat then
2:     Valves connect battery circuit with ED circuit
3:     Pump 1 is active
4:     Pump 2 is active
5:     Fan/Radiator is active
6: else
7:     if T_ED ≥ T_ED && T_bat < T_bat && T_amb < T_out then
8:         Valves disconnect battery circuit from ED circuit
9:         Pump 1 is active
10:        Pump 2 is inactive
11:        Fan/Radiator is active
```

2.3.3 Idling

If all components are in their temperature window, the default setting is "Idling"; all components are in their temperature window, the chiller is turned off, the fan/radiator receives a cooling effect from the vehicle speed and the pumps run on their minimum speed. If T_{amb} is greater than T_{bat} and low battery temperature threshold $\underline{T}_{bat}$ then the valves are closed to the ED circuit. These actions are done in order to prolong temperature increases/decreases. Considering that the coolant flow circulates at a minimum, the flows are still sketched in black (figure 3).

Algorithm 3 Idling

1: **if** $T_{amb} > T_{bat}$ && $T_{amb} > \underline{T}_{bat}$ **then**
2: Valves disconnect battery circuit from ED circuit

2.4 Worldwide harmonized light vehicles test procedure - WLTP

Due to loss of authenticity, the former drive cycle "New European Drive Cycle" (NEDC) needed to be replaced. Experts from the automotive sector as well as politicians from global governments and unions created a new driving cycle - WLTP. It is commonly used by former users of the NEDC.
Since 2017, OEMs have to use the WLTP to certify the emission of their new vehicles. WLTP is supposed to deliver more realistic data to help the customers in their decisions of buying a vehicle. The drive cycle includes more realistic driving scenarios like acceleration and deceleration as well as higher speeds. It will also take into account different vehicle configurations and technologies. Yet, it will not be able to account for individual driving styles and weather conditions. The table below shows a comparison of the former used NEDC and WLTP:

Table 2.1: WLTP/NEDC comparison table[41].

	WLTP	NEDC
Start temperature	23 °C	20 °C to 30 °C
Cycle time	30 minutes	20 minutes
Stationary time proportion	13%	25%
Cycle length	23.25 km	11 km
Speed	Avg.: 46.5 km/h - Max.: 131 km/h	Avg.: 34 km/h - Max.: 120 km/h
Drive power	Avg.: 7.5 kW - Max.: 47 kW	Avg.: 4 kW - Max.: 34 kW

The transition from NEDC to WLTP can cause inflation of the emission values. To prevent this the decision was made to gather real-life data from newly sold vehicles. This will be used to determine the baseline for the aimed emission decrease of 15% in 2025 and 35% in 2030 as illustrated in figure 2.5.

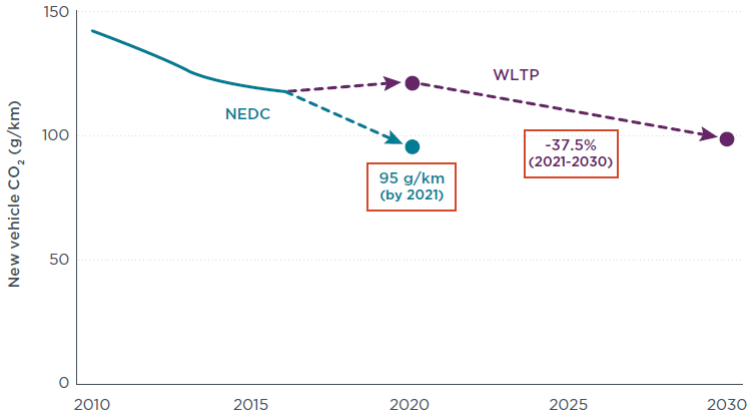

Figure 2.5: Illustration how the CO_2 goal for 2021 is based on NEDC with absolute value of $95 g/km$, while after 2021 a percentage CO_2 reduction applies, relative to WLTP.

Because of the slow inertia of the thermal battery caused by its huge mass, the driving cycle used in this study will be modified and also further referred to as M-WLTP (modified WLTP), see table 2.2.

Table 2.2: M-WLTP initialization data.

	M-WLTP
Ambient temperature	25 °C
Battery temperature	35 °C
Battery coolant temperature	35 °C
Cycle time	110 minutes

The M-WLTP (figure 2.6) includes in the beginning and the end long periods of constant driving. The purpose is to be in a thermally demanding situation for the battery. The current on the battery is comparatively high which increases the battery temperature faster. Nevertheless, the varying driving situations are necessary to present real-world applicability of the controller[5][40].

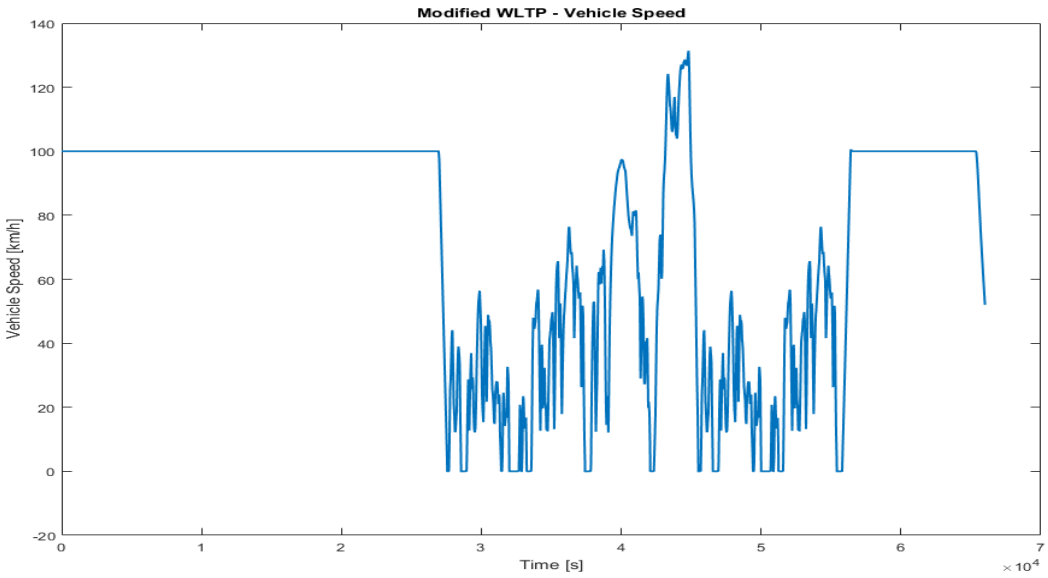

Figure 2.6: M-WLTP drive cycle with a cycle length of 6600s.

2.5 MPC

All MPC algorithms have common components, and it is possible to select distinct alternatives for each component resulting in distinct algorithms: prediction model, objective function, obtaining control law. Figure 2.7 shows a superficial layout. The MPC receives a reference signal r and the output signal of the plant model y. It sends to the plant model the controlling input signal u.

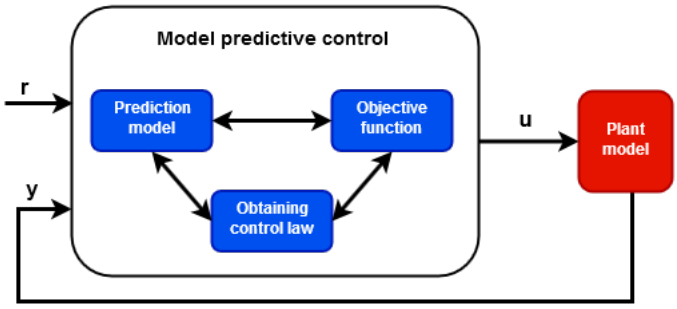

Figure 2.7: A generic model predictive control loop.

2.5.1 Prediction Model

The model is the pillar of MPC; a comprehensive design should include the mechanisms necessary to obtain the optimal model, which should be fully functional to capture the dynamics of the process and allow the predictions to be computed. The need to estimate the predicted output at future instants $\hat{y}(t+k|t)$ determines

the use of the process model. MPC's various approaches can use specific models to portray the connection between outputs and measurable inputs. Those measurable inputs could either be manipulated variables or measured disturbances, atoned by a feedforward-loop. The behaviour can also be influenced by a disturbance model, including non-measurable inputs or noises. Thus, both process and disturbance model complete the prediction model.

2.5.1.1 Process Model

Virtually every form of modeling a process appears in a given MPC formulation. The following being the most widely studied: impulse response, step response, transfer function, state space. As stated in chapter 2.2.3, state space is a convenient and popular solution and will be further demonstrated.

$$\begin{aligned} x(t) &= Ax(t-1) + Bu(t-1) \\ y(t) &= Cx(t) \end{aligned} \tag{2.8}$$

With step time t, state x, input u, output y, and the relevant system matrices A, B, C, D. The prediction with horizon N is calculated with $k = 1, ..., N$ by

$$\hat{y}(t+k|t) = C\hat{x}(t+k|t) = C\Big[A^k x(t) + \sum_{i=1}^{k} A^{i-1} Bu(t+k-i|t)\Big] \tag{2.9}$$

A state space representation offers the benefits of adding multiple variables to a system and estimating the system matrices A, B, C.

2.5.1.2 Disturbance Model

A common disturbance model for state space models are drift disturbances:

$$n(t) = \frac{e(t)}{(1-z^{-1})^2} \tag{2.10}$$

Where $e(t)$ is white noise with a mean of zero and backward shift operator z^{-1}. z^{-1} is the value one time step before t.

2.5.2 Objective Function

Like for the prediction model, the same applies to the cost function regarding the variety. The general objective is that the future output y for prediction horizon P follows the reference trajectory w while the change of control input Δu is penalized:

$$J(P_1, P_2, M) = \sum_{j=P_1}^{P_2} \delta(j)\Big[\hat{y}(t+j|t) - w(t+j)\Big]^2 + \sum_{j=P_1}^{M} \lambda(j)\Big[\Delta u(t+j-1)\Big]^2 \tag{2.11}$$

P_1 and P_2 are the minimum and maximum prediction horizons and M the control horizon; their values are chosen intuitively. A battery plant model requires rather

long prediction horizon, an internal combustion engine is a much faster system and is satisfied with a smaller prediction horizon. δ and λ are the weights of the terms. This way, the engineer can refine the controller's actions by penalizing it. Predictive controls also have the advantage of an a priori knowledge of the system. The reference trajectory $w(t+k)$ can be a close estimation of output y:

$$w(t) = y(t) \tag{2.12a}$$
$$w(t+k) = r(t+k)\alpha^k(y(t) - r(t)) \tag{2.12b}$$

α being a parameter between 0 and 1; small α causes fast-tracking (w_1) and big α a smoother behaviour (w_2) as both cases can be seen in figure 2.8.

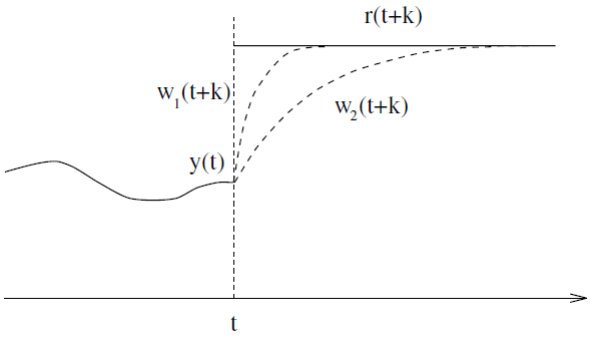

Figure 2.8: Trajectory of reference signal.

Additionally, the cost function is capable of putting constraints on y, u, and Δu. The reasons can be based on economical or physical reasons. Yet, adding constraints increases the complexity of the cost function and must be set cautiously.

$$u_{min} \leq u(t) \leq u_{max} \qquad \forall t \tag{2.13a}$$
$$\Delta u_{min} \leq u(t) - u(t-1) \leq \Delta u_{max} \qquad \forall t \tag{2.13b}$$
$$y_{min} \leq y(t) \leq y_{max} \qquad \forall t \tag{2.13c}$$

2.5.3 Obtaining Control Law

To obtain values $u(t+k)$, the cost function 2.11 must be minimized. For this purpose, the values of the predicted outputs $\hat{y}(t+k)$ are assessed as a function of past input and output values and future control signals, using the model selected and replaced in the cost function, obtaining an expression whose minimization results into the desired values. If the model is linear and without constraints, an analytical solution can be obtained for the quadratic criterion, otherwise an iterative method should be applied. Regardless the procedure, there will be $P_2 - P_1 + 1$ independent variables, which is in the order of around 10 to 30, making it very large. Moreover, this structuralization [42] of the control law generates an

enhancement in the system's robustness and overall behaviour, largely because enabling the free development of the manipulated variables can contribute to undesirable high-frequency control signals and, at worst, to dysfunction. A method to structure the control law is through the use of base functions, which consist of depicting the control signal as a linear combination of certain predetermined base functions:

$$u(t+k) = \sum_{i=1}^{n} \mu_i(t) B_i(k) \tag{2.14}$$

B_i is defined by the process or reference and are typically polynomials

$$B_0 = 1 \qquad B_1 = k \qquad B_2 = k^2 \dots$$

When constraints are set, there are no explicit solutions. Preferably, quadratic programming methods (QP) have to be utilized. For certain types of constraints, however, an explicit solution exists; the condition the output reaches the reference value at a given instant is enforced.

3
Methodology

In this chapter, a workflow is presented which illustrates the methods used during this project. More details of each step are then given in the following sections.

3.1 Workflow

The workflow of this research follows the process illustrated in figure 3.1. This process was developed for the purpose of this study. Yet, it should be applicable on future works.

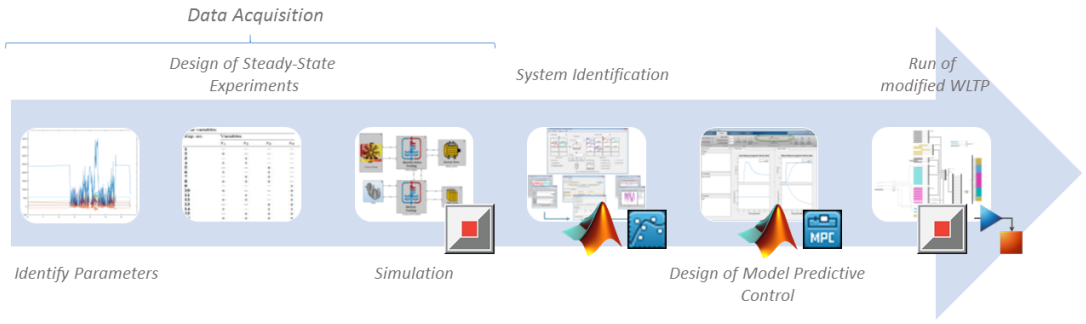

Figure 3.1: Project workflow.

First, the input parameters have to be identified and analyzed. The driving cycle as well as information about operating conditions and energy consumption are given by Volvo Cars. This will aid in planning the correct experiments.

As explained in chapter 2.1, it is fundamental to establish the linear MPC on a linear plant model. Thus, the designed experiments will be in steady-state load conditions with varying cooling influence. These experiments are simulated on a cooling model for a BEV in GT-SUITE, providing realistic results which are based on real-life experiments.

The outcome of those simulation runs are exported then to Matlab. With the support of the System Identification Toolbox (sysID), a state-space representation can be classified which will serve as linear plant model for the Model Predictive Control Toolbox (mpcDesigner).

To conclude, the MPC is connected to the mentioned cooling model for a BEV via a GT-SUITE/Simulink interface model. This allows to use the realistic yet nonlinear GT-SUITE plant model with the multiple linear MPCs.

3.2 Data Acquisition

The data acquisition is split into three sections: parameter identification, design of steady-state experiments and simulation. They yield the further process and without a precise execution, the identification of the system will fail. During the study, it proved itself as a time-consuming task which was surprisingly delicate.

3.2.1 Parameter Identification

In chapter 2.2.3, the equation 2.6 is formulated. The heat rejection $\dot{Q}$ of the components in the electrive drivetrain, the battery current I_{bat} as well as resistance R_{bat} influence the battery's temperature T_{bat}. Simplifications were made for this study; the ED components are viewed as a lumped mass and hence, emit a lumped heat Q_{ED}. The internal battery resistance is a value determined by the GT-SUITE battery model and not an input signal. To fill the structure in 2.5, I_{bat} and Q_{ED} are state parameters in x and the input vector u will consist of the heat from the chiller $Q_{chiller}$ and radiator/fan Q_{fan}. By means of a lookup-table, $Q_{chiller}$ and Q_{fan} will set the correct fan or pump speed to fulfil the request. Figure 3.2 shows relevant parameters: vehicle speed v_{veh}, battery current I_{bat} and lumped heat Q. Additionally, the averages of each with ±50% are plotted.

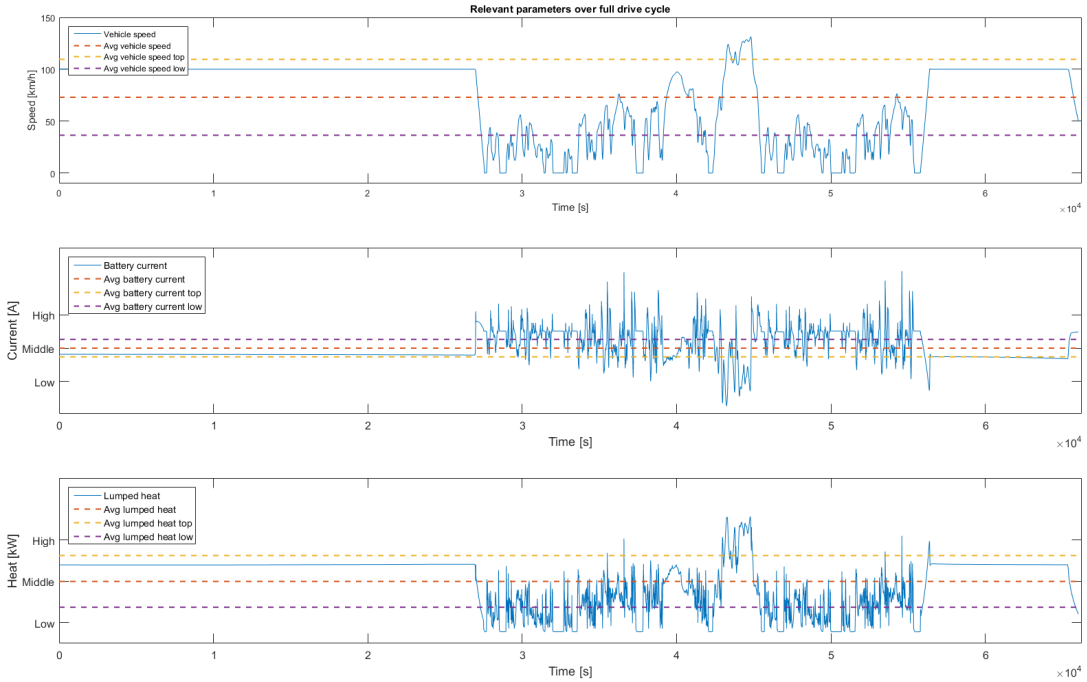

Figure 3.2: Relevant parameters from M-WLTP data.

3.2.2 Design of Steady-State Experiments

Figure 3.2 offers few possibilities on what to focus on for the experiments. First, a full-factorial experiment with three variables p and three levels l which gives 27 experiments n[49]:

$$l^p = n \Rightarrow 3^3 = 27 \tag{3.1}$$

In practice, the simulation duration was about six hours which is too time-consuming. A fractional factorial experiment seems more feasible since the *low/mid/high* load cases seem to be overlaying as can be seen in figure 3.2. This would cut it down to 3 experiments. Considering the thermal modes in chapter 2.3, it can be split in active and passive cooling scenarios as well; the low and high thresholds $T_{bat,Lcrit}$ and $T_{bat,Hcrit}$. This gives then two final steady-state experiments: active cooling, passive cooling. The initial condition of the battery $T_{bat,init}$ will be $T_{bat,Lcrit} < T_{bat,Lcrit} < T_{bat,Hcrit}$ and the indicated high demand case in figure 3.2 will be run.

3.2.3 Simulation

The simulations proceed in GT-SUITE with a cooling system model of a BEV, see figure 3.3. The models are built upon real-life test data and have been approved for accuracy. This guarantees a high quality of the results. The model is fed with the data and the results will be used in the following chapter 3.3.

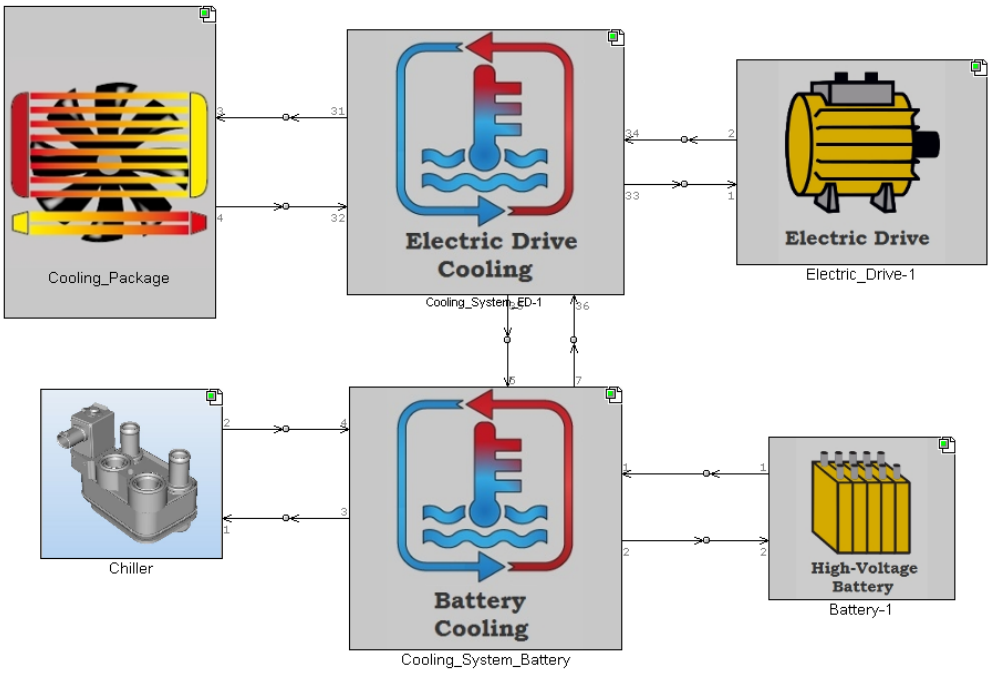

Figure 3.3: Chosen cooling system of BEV in GT-SUITE.

3.3 System Identification Toolbox

Providing input-output data, SYSID is able to build mathematical models of dynamic systems. It identifies continuous-time and discrete-time state-space models, transfer functions, and process models. It allows the user to manipulate the test data and to validate the model against a step response or frequency response.
After importing the data, it will be preprocessed. Analyzing the battery temperature derivative $\dot{T}_{bat}$ (left figure 3.4), the initialization of the model and the high thermal inertia of the battery mass can be obtained. Near steady-state and linearity are desired and thus, the selected range will start at time point $1716s$, see right figure 3.4.

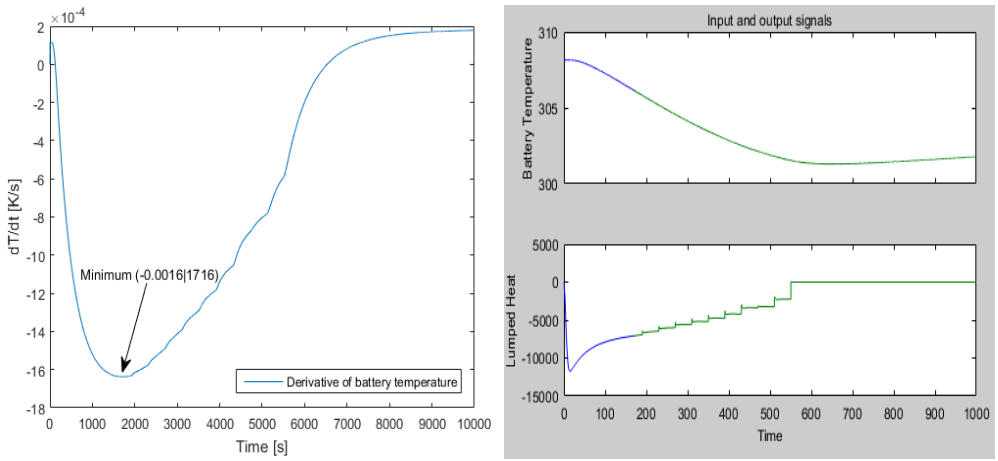

Figure 3.4: Left: derivative of battery temperature; right: preprocessing of input/output data.

The selected data is used then as working and validation data. This is due to the approach from chapter 3.2 where simulations are run for specific cases to design specific MPCs. A state-space model in innovations form is then estimated.

$$\begin{aligned} x(t+1) &= Ax(t) + Bu(t) + Ke(t) \\ y(t) &= Cx(t) + Du(t) + e(t) \end{aligned} \tag{3.2}$$

The same definitions as for equation 2.5 are valid with the addition of matrix K and noise e. The model order can either be specified or a range is given. SYSID plots then a bar-diagram with the singular values (figure 3.5). Singular value shows the contribution of the n'th component of the state vector of the model of order n to the input/output behaviour. A rule of thumb is to select the model order where there is a relatively large drop comparing the left bars to the right bars, usually indicated by a red bar.

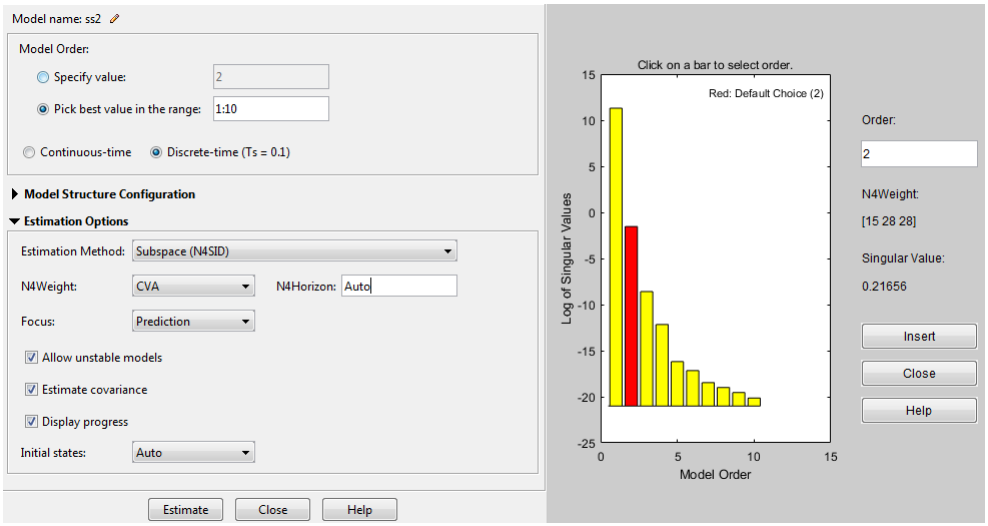

Figure 3.5: State-space estimation via SYSID.

SYSID certifies the selected model against the validation data with a fit of 99.32%; the correlation is this large because the validation and working data are the same. Even though a very efficient and straight-forward tool, it is limited in the sense that the state x cannot be defined and it reconstructed on input u and output y. It delivers a reliable and functioning reduced-order model but with abstract values for the A, B, C, D, K matrices.

```
ss1 =
  Discrete-time identified state-space model:
    x(t+Ts) = A x(t) + B u(t) + K e(t)
       y(t) = C x(t) + D u(t) + e(t)

  A =
                x1           x2
   x1       0.9999  -6.738e-05
   x2   -0.001091       0.9986

  B =
       Lumped Heat
   x1   -1.366e-09
   x2   -2.883e-08

  C =
                          x1          x2
   Battery Temp  2.077e+04      -983.8

  D =
                 Lumped Heat
   Battery Temp             0

  K =
       Battery Temp
   x1       -0.09496
```

```
   x2        -2.006

Name: ss1
Sample time: 0.1 seconds

Parameterization:
   FREE form (all coefficients in A, B, C free).
   Feedthrough: none
   Disturbance component: estimate
   Number of free coefficients: 10
   Use "idssdata", "getpvec", "getcov" for parameters and their ...
       uncertainties.

Status:
Estimated using N4SID on time domain data "actCoole".
Fit to estimation data: 100% (prediction focus)
FPE: 5.659e-12, MSE: 5.648e-12
```

As final step, the model is exported to the workspace where it is augmented via command `ss(ss1,'augmented')` (appendix 3.3). This converts the noise to unmeasured disturbances.

```
ssAug =

  a =
                x1           x2
   x1       0.9999  -6.738e-05
   x2   -0.001091       0.9986

  b =
         Lumped Heat  v@Battery Te
   x1    -1.366e-09    -2.258e-07
   x2    -2.883e-08    -4.769e-06

  c =
                          x1          x2
   Battery Temp  2.077e+04      -983.8

  d =
                   Lumped Heat  v@Battery Te
   Battery Temp              0     2.378e-06

Input groups:
      Name      Channels
    Measured       1
     Noise         2

Name: ss1
Sample time: 0.1 seconds
Discrete-time state-space model.
```

Algorithm 4 System Identification Toolbox

1: Import input&output data
2: Preprocess data: select range, remove trends, etc.
3: Select new data for working data and validation data
4: Estimate state-space model with working data
5: Validate state-space model with validation data
6: Export state-space model to workspace
7: Augment state-space model via ss(ss1,'augmented')

3.4 Model Predictive Control Toolbox

In MPCDESIGNER, it is convenient to start with the application to build first controllers and then to modify them in the further process from the command line. With command line `mpcDesigner` a user-friendly window pops up. Clicking "MPC Structure" grants to select the previously created plant model (figure 3.6).

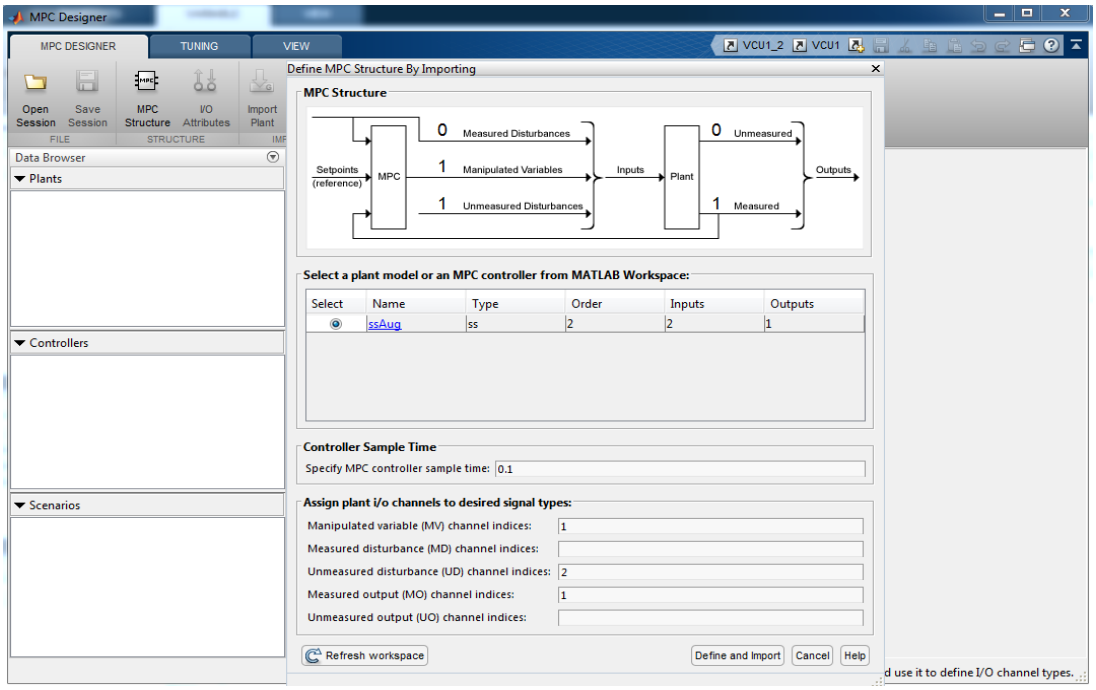

Figure 3.6: Selection of plant model in MPCDESIGNER.

After defining and importing, MPCDESIGNER offers various options. The input/output attributes can be specified. A scale factor is applied if signals have major larger or smaller magnitudes than the others. The weight tuning also benefits from reasonable scale factors. The scale factor can be defined by the upper and lower limit of the respective signal. Are the limits unknown, open-loop simulation with varying the inputs over a likely range can provide the limits. The nominal value of the input/output signals can also be assigned; at these values the plant model was linearized.

With "Edit Scenario", the scenario settings can be adjusted; the reference signal can vary from "Step", "Ramp" or to none "Constant", the simulation time can be changed and disturbances added. In "Tuning", the sample time, prediction horizon and control horizon can be defined. Since the battery is a relatively slow system, generous times are selected: the prediction horizon is 200s and the control horizon is 30s. To reduce the computational time, the sample time is set at 10s even though the MPC will be connected with the GT-SUITE model which has a sample time of 0.1s. With a rate transition block in SIMULINK this difference can be taken care of. By default, it transfers deterministic data with no random values. Physical limitations are set in "Constraints". The unmeasured disturbance will be specified as a white noise with a static gain of one. Eventually, the weights are applied. Both rate of value change and magnitude of value can be penalized. Since an energy efficiency increase is desired, the rate will be more penalized than the absolute value. The control behaviour on a step signal can be seen in figure 3.7

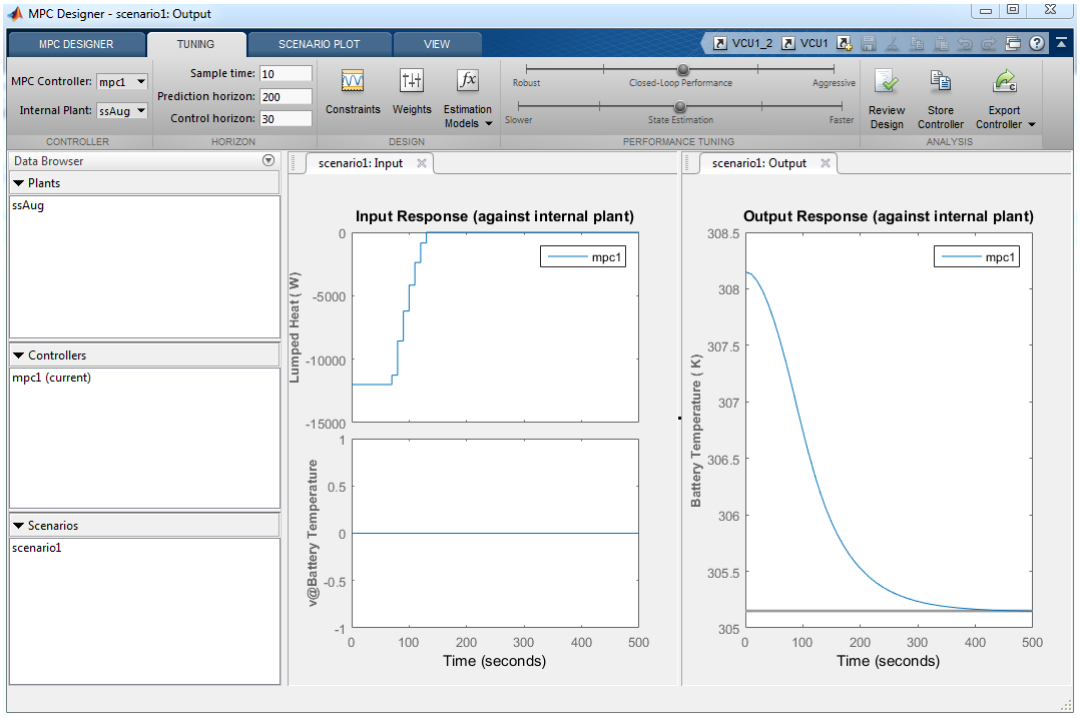

Figure 3.7: Step signal on MPC in MPCDESIGNER.

The right plot shows the battery temperature being cooled down to the reference temperature. The control input is plotted next to it. Since the sample time is set at 10s, the input signal shows an incremental behaviour. When the controller has a satisfying response, a SIMULINK model can be generated with the control, plant and reference, figure 3.8.

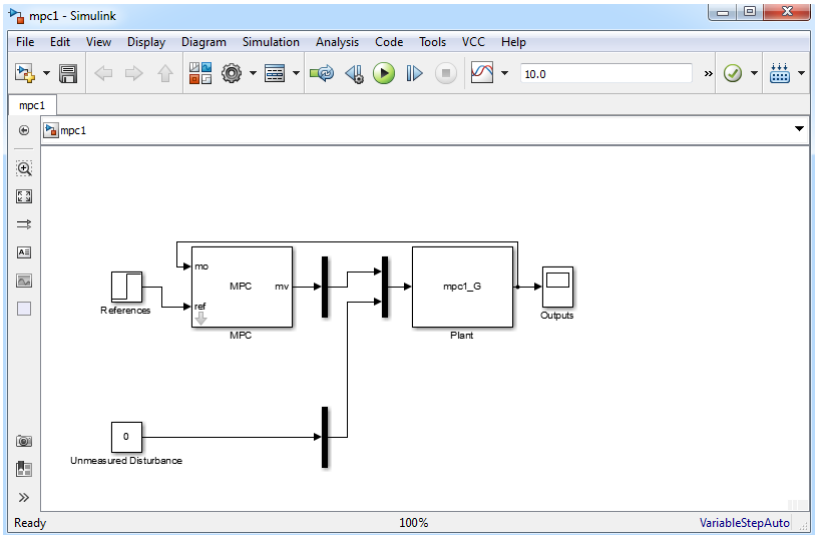

Figure 3.8: MPC exported to SIMULINK.

3.5 GT-SUITE/Simulink Interface

In figure 3.9, the GT-SUITE/SIMULINK interface model is displayed with SIMULINK as master. The MPC is connected via a GT-SUITE as slave block which refers to a `.dat`-file. This `.dat`-file is generated in GT-SUITE from the complete cooling model of the BEV. SIMULINK as master feeds the GT-SUITE model with input data as the vehicle speed or ambient temperature but also the control input signals u for the various pump speeds and valve openings/closings. In return, GT-SUITE sends each time step the output data y to the predictive control.
For this interface, a harness of the input and output signals has to be designed in GT-SUITE. It is crucial that the signal names and signal order in GT-SUITE match the signal names and signal order in SIMULINK. Additionally, all signals to GT-SUITE have to be of datatype double and a rate transition has to be implemented either by blocks from the SIMULINK library or by checking the box "Automatically handle rate transition for data transfer" in $ModelExplorer \Rightarrow Configuration(Active) \Rightarrow Solver$. These modifications enable then the connection of multiple linear MPCs to work with the nonlinear plant model from GT-SUITE.

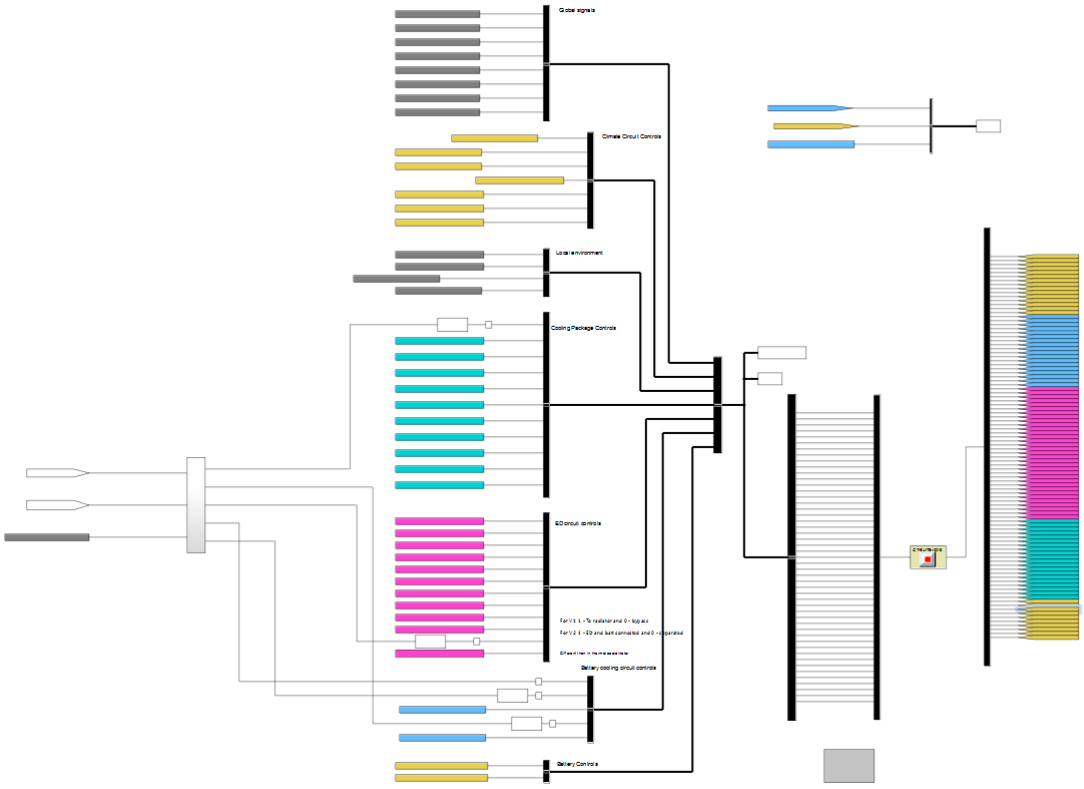

Figure 3.9: GT-SUITE/Simulink interface model.

3.5.1 Fine-Tuning of MPC

As discussed in the literature review (chapter 2.1), Huang et al. [15] design a hybrid predictive control which utilizes the benefits of on/off-controls and model predictive controls. On/off-controls tend to oscillate between upper and lower boundaries whereas MPCs are active to prevent slightest violations of the target; both habits are energy-consuming and can easily be eliminated by combining the controllers. The thermal modes in chapter 2.3 will be the base of the switch-logic which picks the correct thermal mode. Input will be the significant temperatures and vehicle speed.

3.5.2 Classic Control

The classic control is based on multi-level on/off-controllers which rely on look-up tables and the switch-logic introduced in the previous section 3.5.1. The correct thermal mode is selected according to battery and ED temperature. The vehicle speed is fed as well to select the correct fan speed; this structure makes it a coupled control with feedback and feed-forward input.

4

Results

All the following plots are generated from the classic control and the predictive control using the modified WLTP drive cycle from chapter 2.4. The simulation runs of both controls will be presented and with each other compared. Their contrast in performance will be pointed out in plots which show the data of interest. Brief discussions of the results are accompanied with the plots. Last, an analysis completes this chapter.

4.1 Temperature

Figure 4.1 shows the battery temperature during the M-WLTP drive cycle. The MPC is able to reach its target of $306°K$ faster but has a larger undershooting. The classic control follows the target value closer than the MPC. However, the MPC violates the target value less than the classic control, see table 4.1. Comparing the complete drive cycle, the MPC violates the target value 29.33% compared to 34.39%. A cut drive cycle is also considered where the focus is on $1300 - 6600s$ of the M-WLTP. Ergo, the temperatures are below the target value and it demonstrates each controls quality. Here, the MPC achieves the lower violation as well with 16.44% againts 18.73%. In total, the MPC violates the target value 11 times while the classic control violates it 16 times.

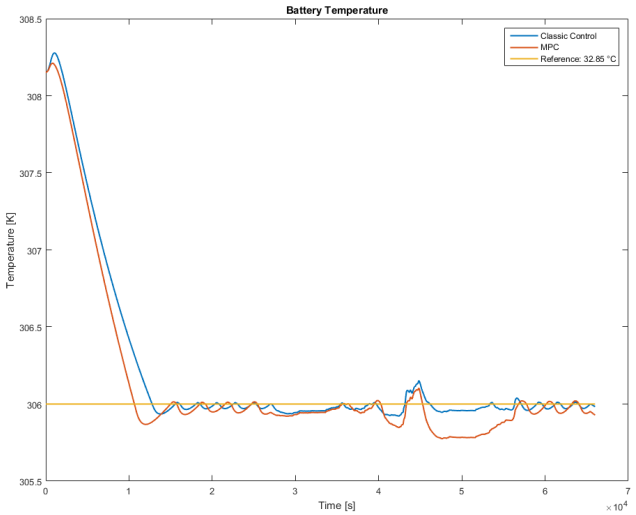

Figure 4.1: Battery temperature.

Table 4.1: Violation of target temperature.

	MPC	Classic
M-WLTP	29.33%	34.39%
Cut M-WLTP	16.44%	18.73%

The conclusion from chapter 2.2.2 where a greater ΔT is achieved with a warmer inlet temperature to the fan can be confirmed by the simulations as well (figure 4.2). This offers big potential in saving energy but needs further investigation for implementation since the temperature limitations of the ED components have not been fully researched.

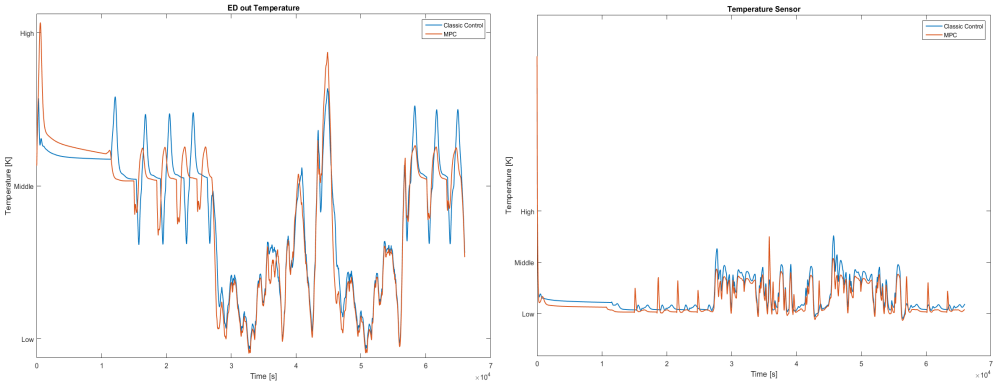

Figure 4.2: Left: ED component temperature; right: temperature from temperature sensor.

4.2 Thermal Modes and Input Signals

Correlating the speed profiles from the right plot in figure 4.4 and the plots from figure 4.3 attests the predictive nature of the MPC; the speed varies more in the behaviour and reduces the speed if possible to save energy which is due to the cost function. Yet, the undershootings are greater than from the classic control. This needs further fine-tuning which would result into further energy savings.

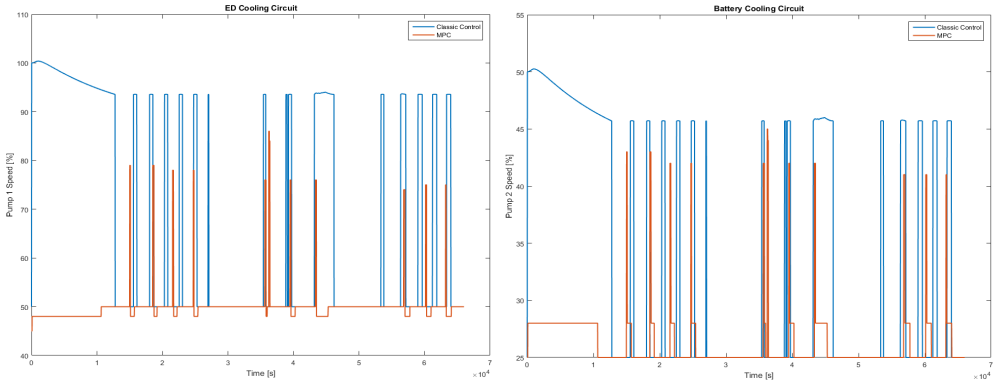

Figure 4.3: Left: ED circuit pump speed; right: battery circuit pump speed.

The thermal modes in the left plot of figure 4.4 show the habit of the hybrid-control. For comparison reason, both the predictive and classic control work with the same threshold for each thermal mode. More adjustments to the switch-logic would enhance the MPC even more as would the classic control. Thus, both are given the same switch-logic.

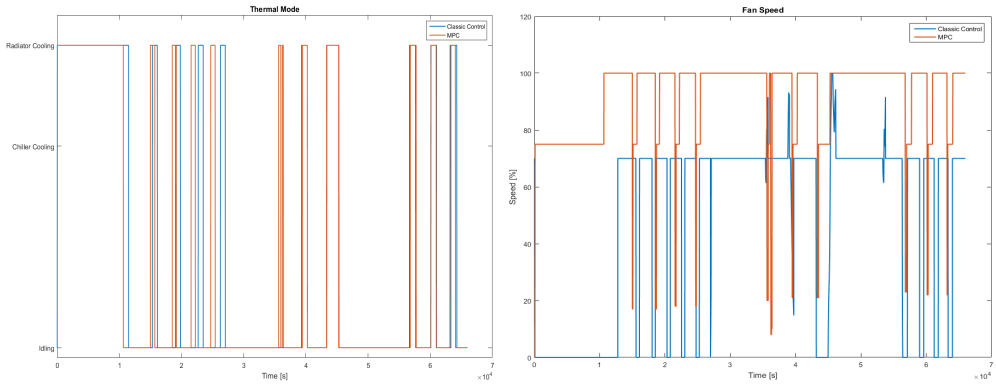

Figure 4.4: Left: thermal modes; right: fan speed.

4.3 Energy Consumption

The energy consumption of all energy consumers of the complete vehicle are evaluated and plotted in figure 4.5; the left side is for the complete drive cycle, the right side for the cut drive cycle, the top is the energy at the time instant, the bottom the accumulated energy consumption. The figure at the top correspond to the speed profiles in figure 4.3 and 4.4 and the continual increase of energy consumption is due to the minimum speed requests.

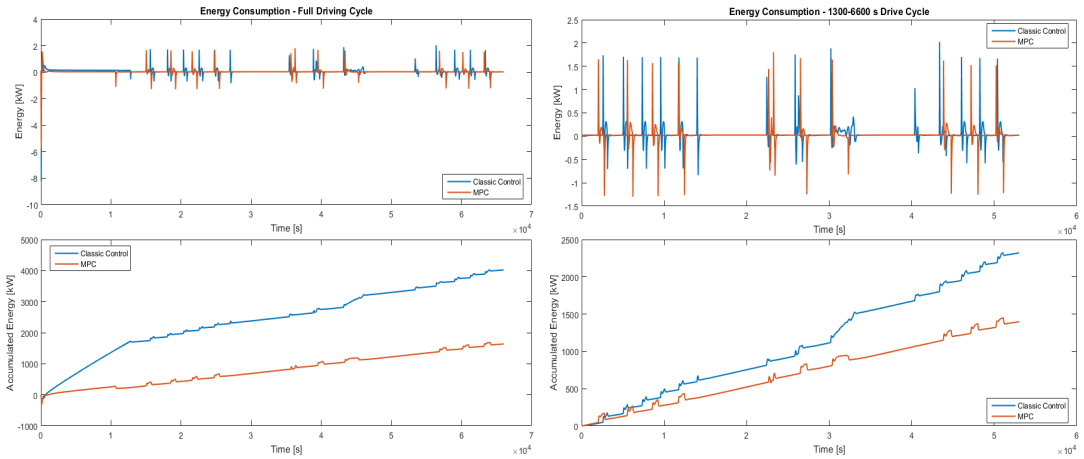

Figure 4.5: Left: energy consumption of complete WLTP; right: energy consumption of cut WLTP.

The bar 4.6 exposes the improvement achieved if a predictive control is utilized. For the complete WLTP drive cycle, the energy consumption is decreased by 59.29%. As noticed, the initialization period is very demanding and fine-tuning of the classic control would diminish this steep increase (bottom left plot in figure 4.5). Hence, the drive cycle is trimmed to the $1300 - 6600s$ period and further analyzed. Still, a great decrease of 39.75% can be realized.

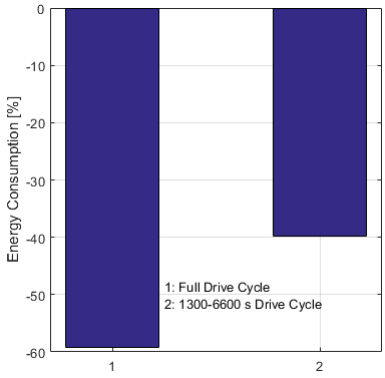

Figure 4.6: Comparison of drive cycles.

	M-WLTP	Cut M-WLTP
Classic	4.02 kW	2.32 kW
MPC	1.64 kW	1.40 kW
Benefit	-59.29%	-39.75%

Table 4.2: Energy consumption.

4.4 Analysis

The predictive control proves itself to be notably robust and adaptable. The M-WLTP drive cycle varies the load conditions continuously and still, the MPC manages to apply inputs u which prevent violations of the target temperature less often in both quantity and duration than the classic control, figure 4.1. The more variable speed profile of the pumps and fan indicate the smarter control which result into a grand energy reduction, figures 4.3 and 4.4. Yet, the MPC undershoots the reference temperature more often than the classic control. If the MPC would have similar magnitudes of the undershoot as the classic control, the energy consumption would decrease again significantly. The huge undershoot of the battery temperature around $4500s$ in figure 4.1 is the result of a change from a high-demanding to a low-demanding load, see M-WLTP drive cycle figure 2.6. A better implementation of the load and a bigger prediction horizon could eliminate this temperature drop. Nonetheless, comparing the pump speeds (figure 4.3) at these time stamps show that the both speeds adjust for the change in load whereas the classic control drives relatively high speeds. Moreover, the oscillations of both controls is due to the switch-logic which needs further adjustments. A closer accompaniment of the target is associated with a higher energy consumption since the pumps are not idling but active. Alternatively, the boundaries of the switch-logic can be adapted to allow for more movement between the upper and lower limitations.

5
Conclusion

The goal of this research was the investigation of the potential of a predictive control for the battery thermal management of a battery-electric vehicle. The control strategy is compared to a traditional controller using Simulink in connection with a cooling system model in GT-SUITE. The benefit of this interface is that the plant model does not need to be designed in advance but the GT-SUITE model serves as it. Also, the GT-SUITE model is based on real-life test data making the simulation results very credible. From a control engineer's perspective, it is a preferred choice to work with Matlab and Simulink on account of convenience and available functions. On the contrary, the plant model is nonlinear and can make the designing of the predictive control highly complicated. Another drawback is that in this context, the possibility of real-life applicability cannot be examined since the GT-SUITE model has a high computational time by virtue of the complexity of the cooling system model. Hence, a method had to be established which utilizes the benefits of the genuine GT-SUITE model and the functionality in Simulink.
During the literature review, I became aware of the variety and complexity of this topic. The model predictive control is available in many forms, linear- or nonlinear-based. Albeit, both principles have been studied, the implementation of a nonlinear MPC did not seem feasible. An alternative has been developed and similar solution have been published, see [51]. Ergo, owing to the complexity of the task an approach through linearizing the non-linear conditions was not only necessary but the use of reduced-order models is actually more beneficial; it is less computational heavy and the discrepancy between predicted output and actual output is minimized en passant since the prediction is computed each time step. Building a control based on high load cases proved itself as sufficient for the M-WLTP drive cycle with varying load cases, although, it could be characterized as conservative. Nevertheless, an improvement has been achieved.
However, the comparison lacks quality on side of the base model. The traditional control has not experienced the same amount of dedication as the MPC which is more sophisticated; the large improvement in energy consumption seems implausible and not sound. It has been tried to compensate for this but time is scarce and valuable and cannot be replaced.
The investigation was accompanied by many challenges and unknowns. Contrary to my expectations, not the designing of the model predictive control was the most time-consuming but the constructing of the plant model as is also indicated in research papers. Developing an appropriate method for this context

required the examination of various approaches. To conclude this study, the developed method demonstrated a positive realization and the results indicate a high potential.

6
Future Work

The increase of interest in predictive control is steadily growing and with the possibilities of vehicle-to-everything (V2X) communication, the possibilities are immense. A control engineer's dream is a perfect foreknowledge of the control environment. In [18], the authors demonstrate the potential of V2V (vehicle-to-vehicle) and V2I (vehicle-to-infrastructure) technology in combination with an MPC. Many more examination of this topic have been tuned for real-life applications and confirmed the potential. Consequently, the extension of the inspected BEV model (figure 2.2) to a complete cooling system including the A/C system is recommended in order to finalize the thermal management. The integration of available cloud data in the thermal management and unlocking their full potential has shown significant improvements.
Yet, this controller needs to perform at a low computational cost, otherwise, real-life applications are not feasible. Most likely, the strategy of this study has to be adjusted and a dissociation of MATLAB is inevitable. New challenges will occur; the implementation on a vehicle's ECU can be very tedious regarding OEM specific data types of ECU signals, for example.
Moreover, the GT-SUITE/SIMULINK interface model has been a very valuable tool. The possibility of testing the control in extensive simulations is fairly unique but very effective; control strategies can be tested in an authentic and realistic environment and hence, accelerating the development process of control strategies immensely. With an utilization of an entire vehicle model in GT-SUITE the quality of the simulation would even further increase. Developing time of the control can be spend more independent from the development status of the vehicle and changes can be easily applied and simulated.

Bibliography

[1] Council of the European Union (2018) - "Proposal for a Regulation of the European Parliament and of the Council setting emission performance standards for new passenger cars and for new light commercial vehicles as part of the Union's integrated approach to reduce CO2 emissions from light-duty vehicles and amending Regulation (EC) No 715/2007", Interinstitutional File: 2017/0293(COD)

[2] NASA's Goddard Institute for Space Studies. URL: `https://climate.nasa.gov/` (accessed: 19.05.2019)

[3] Dincer, I., Midilli, A., Hepbasli, A., Karakoc, T. H.; Global Warming: Engineering Solutions. Springer (2010)

[4] Ritchie, H., Roser, M. (2019) - "CO_2 and other Greenhouse Gas Emissions". URL: `https://ourworldindata.org/co2-and-other-greenhouse-gas-emissions` (accessed 19.05.2019)

[5] International Council on Clean Transportation (2019) - "CO_2 Emission Standards for Passenger Cars and Light-Commercial Vehicles in the European Union"

[6] Seibt, T. (2019) - "Neuzulassungen Elektro-Autos April 2019 (German) [New registration of electriv vehicles April 2019". URL: `https://www.auto-motor-und-sport.de/verkehr/elektroauto-neuzulassungen-deutschland-april-gesamtjahr-2019/` (accessed 19.05.2019)

[7] Artstein, Z. (1980) - "Discrete and Continuous Bang-Bang and Facial Spaces or: Look for the Extreme Points". URL: `https://www.jstor.org/stable/2029960` (accessed 19.05.2019)

[8] Khaled, N., Pattel, B.; Practical Design and Application of Model Predictive Control. Elsevier (2018)

[9] Araki, M. (1980) - "CONTROL SYSTEMS, ROBOTICS, AND AUTOMATION – Vol. II - PID Control". Princeton University Press. ISBN 9780691653259.

[10] Flügge-Lotz, I. (1953) - "Discontinuous Automatic Control". URL: http://www.eolss.net/ebooks/Sample 20Chapters/C18/E6-43-03-03.pdf (accessed 19.05.2019)

[11] Seborg, D., Edgar, F., Mellichamp, D.; Process Dynamics and Control. John Willey & Sons (2004)

[12] Camacho, E. F., Bordons, C.; Model Predictive Control. Springer (2007)

[13] del Re, L., Allgöwer, F., Glielmo, L., Guardiola, C., Kolmanovsky, I.; Model Predictive Control. Springer (2010)

[14] Kouvaritakis, B., Cannon, M.; Model Predictive Control - Classical, Robust and Stochastic. Springer (2016)

[15] Huang, Y., Khajepour, A., Bagheri, F., Bahrami, M.; Optimal energy-efficient predictive controllers in automotive airconditioning/refrigeration systems. Applied Energy (2016);184:605–618

[16] Traussnig, A., Stolz, M., Horn, M.; MPC based Fan Control for Automotive Applications. IFAC (2016).

[17] Liu, Y.; Robust Nonlinear Control Design with Proportional-Integral-Observer Technique. Universität Duisburg-Essen (2011).

[18] Amini, M. R., Sun, J., Kolmanovsky, I.; Two-Layer Model Predictive Battery Thermal and Energy Management Optimization for Connected and Automated Electric Vehicles. 57th IEEE Conference on Decision and Control (2011).

[19] Lim, H., Su, W., Mi, C.; Distance-Based Ecological Driving Scheme Using a Two-Stage Hierarchy for Long-Term Optimization and Short-Term Adaptation. IEEE Trans. on Vehicular Technology, 66(3):1940–1949 (2017).

[20] Bauer, S., Suchaneck, A., León, F. P.; Thermal and energy battery management optimization in electric vehicles using Pontryagin's maximum principle. Journal of Power Sources, 246:808–818 (2014).

[21] Sun, C., Sun, F., Hu, X., Hedrick, J., Moura, S.; Integrating traffic velocity data into predictive energy management of plug-in hybrid electric vehicles. In ACC (2015).

[22] Herrera, J., Work, D., Herring, R., Ban, X., Jacobson, Q., Bayen, A.; Evaluation of Traffic Data Obtained via GPS-Enabled Mobile Phones: The Mobile Century field experiment. Transportation Research Part C: Emerging Technologies, 18(4):568–583 (2010).

[23] Fischer, T., Götz, F., Berg, L., Kollmeier, H.-P., Gauterin, F.; Model-based development of a holistic thermal management system for an electric car with a high temperature fuel cell range extender. 11th Int. Modelica Conference (2015).

[24] Fischer, T., Kraus, T., Kirches, C., Gauterin, F.; Nonlinear Model Predictive Control of a Thermal Management System for Electrified Vehicles using FMI. 12th Int. Modelica Conference (2017).

[25] Cengel, Y. A., Boles, M. A.; Thermodynamics: An Engineering Approach. Mcgraw-Hill College (2008).

[26] Howell, J. R., Buckius, R. O.; Fundamentals of Engineering Thermodynamics. Mcgraw-Hill College (2008).

[27] Central-Air-Conditioner-and-Refrigeration.com; Refrigeration Cycle Explained in Easy Way. URL: `http://www.central-air-conditioner-and-refrigeration.com/Refrigeration_Cycle.html` (accessed: 19.05.2019).

[28] Berg Chilling Systems Inc.; URL: `https://berg-group.com/engineered-solutions/the-science-behind-refrigeration/` (accessed: 19.05.2019).

[29] Stanford III, H. W.; HVAC Water Chillers and Cooling Towers - Fundamentals, Application, and Operation Second Edition. Taylor & Francis Group (2012).

[30] Rao, Y. V. C.; An Introduction to Thermodynamics. Sangam Books Ltd. (2004).

[31] Hu, X., Lin, S., Stanton, S., Lian, W.; A State Space Thermal Model for HEV/EV Battery Modeling. ANSYS Inc. (2011).

[32] Volvo Car Group; URL: `https://www.volvocars.com/uk/about/human-innovation/future-of-driving/fuel/electric-cars` (accessed 19.05.2019).

[33] Volvo Car Group; URL: `https://www.media.volvocars.com/global/en-gb/media/pressreleases/252485/volvo-car-group-signs-multi-billion-dollar-battery-supply-deals-with-catl-and-lg-chem` (accessed 19.05.2019).

[34] Bandhauer, T. M., Garimella, S., Fuller, T. F.; A Critical Review of Thermal Issues in Lithium-Ion Batteries. Jouranl of The Electrochemical Society (2011).

[35] Chen, Y., Song, L., Evans, J.; Modeling Studies on Battery Thermal Behaviour, Thermal Runaway, Thermal Management, and Energy Efficiency. Proceedings of Energy Conversion Engineering Conference, the 31st Intersociety, volume 2 (1996).

[36] Kiehne, H.; Battery Technology Handbook. CRC Press (2003).

[37] Linden, D., Reddy, T.; Handbook of Batteries. Mcgraw-Hill College (2002).

[38] Schilders, W.,H., van der Vorst, H. A., Rommes, J.; Model Order Reduction: Theory, Research Aspects and Applications. Springer (2008).

[39] Bernardi, D., Pawlikowski, E., Newman, J.; A General Energy Balance for Battery Systems. ECS (1985).

[40] Volvo Car Group; URL: `https://www.volvocars.com/international/own/explore/eu-emission-tests` (accessed 19.05.2019).

[41] Volvo Car Group; URL: `https://www.volvocars.com/intl/own/explore/eu-emission-tests/wltp-vs-nedc` (accessed 19.05.2019).

[42] De Keyser, R. M. C.; Basic Principle of Model Based Predictive Control. 1st European Control Conference, Grenoble, pages 1753–1758 (1991).

[43] Erjavec, J.; Automotive Technology - A Systems Approach. Thomson Delmar Learning (2005).

[44] Zhang, Q., Li, S. E., Deng, K.; Automotive Air Conditioning - Optimization, Control and Diagnosis. Springer (2016).

[45] Theodore, L.; Heat Transfer Application for the Practicing Engineer. John Wiley & Sons (2011).

[46] Schütz, T.; Hucho - Aerodynamik des Automobils: Strömungsmechanik, Wärmetechnik, Fahrdynamik, Komfort. Springer (2013).

[47] Google Ngram Viewer; URL: `https://books.google.com/ngrams/info` (accessed 19.05.2019).

[48] Kim, E., Lee, J., Shin, K. G.; Real-Time Battery Thermal Management for Electric Vehicles. University of Michigan (2014).

[49] Lundstedt, et al.; Experimental design and optimization. Chemometrics and Intelligent Laboratory Systems (1998).

[50] Weiss, C.; URL: `http://www.charles-hatchett.com/public/images/documents/2018/cedric_weiss_electric_vehicle_battery_chemistry_and_pack-architecture.pdf` (accessed 29.05.2019).

[51] Chen, R., Maloney, P.; URL: `https://se.mathworks.com/videos/model-predictive-control-of-diesel-engine-airpath-81995.html` (accessed 29.05.2019).